NASA CONTRACTOR
REPORT

NASA CR-61341

# DEVELOPMENT OF OPTICAL DATA PROCESSING TECHNIQUES APPLICABLE TO DETECTION AND STUDY OF METEOR TRAILS

By T. H. Gee, C. W. Allen, and S. M. Amin
The University of Tennessee Space Institute
Tullahoma, Tennessee

December 1970

Final Report



Prepared for

NASA-GEORGE C. MARSHALL SPACE FLIGHT CENTER
Marshall Space Flight Center, Alabama 35812

| 1. Report No. | 2. Government Accession No. | 3. Recipient's Catalog No. |
|---|---|---|
| NASA CR-61341 | | |

| 4. Title and Subtitle | 5. Report Date |
|---|---|
| DEVELOPMENT OF OPTICAL DATA PROCESSING TECHNIQUES APPLICABLE TO DETECTION AND STUDY OF METEOR TRAILS | December 1970 |
| | 6. Performing Organization Code |

| 7. Author(s) | 8. Performing Organization Report No. |
|---|---|
| T. H. Gee, principal investigator<br>C. W. Allen, S. M. Amin, graduate research assistants | |
| | 10. Work Unit No. |
| 9. Performing Organization Name and Address<br>The University of Tennessee Space Institute<br>Tullahoma, Tennessee | 11. Contract or Grant No.<br>NAS 8-24393 |
| | 13. Type of Report and Period Covered<br>Final<br>Contractor Report |
| 12. Sponsoring Agency Name and Address<br>National Aeronautics and Space Administration<br>Washington, D. C. 20546 | 14. Sponsoring Agency Code |

15. Supplementary Notes

Prepared for George C. Marshall Space Flight Center
Marshall Space Flight Center, Alabama 35812

16. Abstract

An investigation has been conducted which was directed towards development of coherent optical data processing techniques applicable to detection of meteor trails and subsequent study of their properties. The coherent optical matched filter was chosen for implementation of such a system. The matched filter was studied with regard to its selectivity and output light distribution as a function of the bandpass characteristics of the filter. Exposure and processing of photographic film, the matched filter recording medium, were experimentally studied to determine the important parameters affecting filter operation. This included addition of a bleaching step to the film processing procedure for improved filter diffraction efficiency.

Various bandpass conditions were experimentally established by varying the exposure of the film to the signal component during filter formation. Experiments were conducted relevant to meteor trail detection, and rejection of star images, using a modified closed circuit television system to provide an output plane detector and readout device. Results of these efforts led to specifications and design criteria for an optical data processing system for meteor trail detection and study.

| 17. Key Words (Suggested by Author(s)) | 18. Distribution Statement |
|---|---|
| | Unclassified - unlimited<br>John K. Williams |

| 19. Security Classif. (of this report) | 20. Security Classif. (of this page) | 21. No. of Pages | 22. Price* |
|---|---|---|---|
| Unclassified | Unclassified | 101 | $ 3.00 |

*For sale by the National Technical Information Service, Springfield, Virginia 22151

TABLE OF CONTENTS

## LIST OF SYMBOLS

| | |
|---|---|
| A | amplitude of reference beam |
| a | x dimension of rectangular aperture input signal |
| a′ | x dimension of rectangular aperture to which filter is matched |
| b | y dimension of rectangular aperture input signal |
| b′ | y dimension of rectangular aperture to which filter is matched |
| D | film density |
| d | separation of transform lens and filter plane (Fig. 26) |
| $E_r$ | exposure due to reference beam component |
| $E_s$ | exposure due to signal component |
| $f_1$ | focal length of transform lens |
| $f_2$ | focal length of transform lens |
| G | signal to which filter is matched |
| I | intensity distribution |
| i | $\sqrt{-1}$ |
| K | light amplitude illuminating input plane |
| k | $2\pi/\lambda$ |
| m | upper cut off frequency in x dimension |
| m′ | lower cut off frequency in x dimension |
| n | upper cut off frequency in y dimension |
| n′ | lower cut off frequency in y dimension |
| S | input signal |
| S/R | signal to reference component intensity ratio |
| T | amplitude transmission factor |

| | |
|---|---|
| $U$ | light amplitude distribution |
| $u$ | $x_2/\lambda f_1$ |
| $v$ | $y_2/\lambda f_1$ |
| $x_1, y_1$ | input plane coordinates |
| $x_2, y_2$ | frequency or filter plane coordinates |
| $x_3, y_3$ | output plane coordinates |
| $z_1$ | separation of filter plane and transform lens (Fig. 26) |
| $z_2$ | separation of transform lens and output plane (Fig. 26) |
| $\alpha$ | spatial frequency, sin $\theta/\lambda$ |
| $\gamma$ | photographic film gamma |
| $\epsilon$ | output plane scale factor (Appendix B) |
| $\theta$ | angle which reference beam makes with the optic axis |
| $\lambda$ | wavelength of monochromatic light |
| $\rho$ | diameter of circular aperture input signal |
| $\Phi$ | correlation function |
| $\sim$ | denotes Fourier transformation |
| * | denotes complex conjugate |

# CHAPTER I

## INTRODUCTION

One of the more modern approaches to the problem of pattern recognition utilizes techniques of coherent optics to perform correlation analyses. An investigation directed towards development of coherent optical data processing techniques applicable to detection and study of meteor trails has been conducted at The University of Tennessee Space Institute under sponsorship of The National Aeronautics and Space Administration's Marshall Space Flight Center/Space Sciences Laboratory. This report presents theoretical and experimental findings from these research efforts.

Implementation of a coherent optical data processor for pattern recognition purposes can be effected by use of the matched filter, a complex filter which is made to detect a particular signal (generally, a two-dimensional signal) in the presence of other signal forms and noise. Basic to the research efforts reported here is the assumption that meteor information is collected and made available to the optical system by means of photographic film transparencies. Thus, the matched filter must be capable of detecting the presence of meteor trails while rejecting star

images and other forms of noise. Techniques and applications of matched filter pattern recognition appear in the open literature (1,2,3,4,5).* An analysis and discussion of a coherent optical matched filter system is presented in Appendix A of this report.

As shown in Appendix A, operation of the matched filter is essentially that of performing a correlation analysis between two signals; one signal is an input to the system and the second is a signal to which the filter is matched. The output of such a system is a light intensity distribution proportional to the squared magnitude of the resulting correlation function. Thus, the detectable output quantity is a measure of the similarity between a known and an unknown signal.

Important aspects of matched filter operations which have been investigated during the period of this contract include characterization of the matched filter with regards to its selectivity and output light distribution, determination of factors influencing filter diffraction efficiency, and an investigation of the effects of input signal format contrast. In addition, a matched filter optical configuration which affords operational advantages in meteor trail

---

* Numbers in parentheses refer to similarly numbered references in the bibliography.

detection has been designed. Experiments have been conducted to determine the limitations of the theory employed and to demonstrate the practicability of optical data processing techniques, as applied to meteor trail studies.

An important consideration here concerns the manner in which the matched filter distinguishes between similar signals. It has been shown that certain steps can be taken in matched filter formation to improve the ability of a filter to distinguish between similar signals (6). In this regard, an appropriate matched filter model has been studied, both from a theoretical and experimental viewpoint, to determine parameters affecting filter selectivity as well as to characterize practical matched filter operation. It is shown that the matched filter's bandpass characteristics determine its selectivity and the output light distribution. This study is presented as Chapter II. A narrow rectangular aperture was employed as a meteor trail model in these studies. An expression for the output light distribution (correlation intensity) corresponding to rectangular signal formats is developed and presented in Appendix D.

Typical hologram diffraction efficiencies are two to three percent. Since the matched filter is in fact a Fourier transform hologram, detection of the matched filter output is affected by its diffraction efficiency. Experiments were conducted to determine the proper matched filter film (or

photographic plate) density which would yield a relatively high diffraction efficiency. Borrowing from the experience of holographers, a bleaching step was added to the film processing procedure. The effects of film bleaching were studied to determine the manner in which bleaching affects matched filter operation. It was found that matched filter efficiencies can be improved by proper bleaching. Also, the selectivity exhibited by unbleached filters is decreased after bleaching. These studies are presented and discussed in Chapter III.

Chapter IV consists of discussions and experimental results relevant to the effects of input signal format contrast upon the operation of matched filters. This is one of the more important factors in the use of matched filter techniques for detection of meteor trails because the input signals are recorded on photographic film with typically low contrast between the signal and the signal background. The contrast is dependent upon the properties of the meteor (size and etc.) entering the earth's atmosphere and the characteristics of the film on which these images are recorded. Effects of input signal (meteor trail) rotation as a function of filter selectivity are also considered in Chapter IV. Finally, the ability of the matched filter to discriminate against circular aperture type formats (representative of star images) is considered.

The design of a coherent optical matched filter system is presented and discussed in Chapter V. An analysis of this system appears in Appendix B. This system consists of a spherical wave matched filter correlator which was designed to minimize the number of lenses employed, subsequently minimizing the system noise introduced by the lenses. Such a system also provides a transform plane scaling capability which allows similar input signals to be scaled to a single matched filter. Several output detection schemes are considered in the system design, and a closed circuit television line scanner and visual monitor design is given in Appendix C.

Finally, Chapter VI includes conclusions drawn from these research efforts and recommendations for implementing the various techniques reported here.

# CHAPTER II

## OPERATION OF THE MATCHED FILTER AS A FUNCTION OF ITS BANDPASS CHARACTERISTICS

In this chapter, the operation of the matched filter as a function of its bandpass characteristics is considered. In particular, the effects of filter bandpass characteristics upon the filter selectivity, or ability to distinguish between similar signals, and the output correlation light distribution have been investigated.

### Physical Significance of Bandlimiting

In general, the energy density spectrum of a signal reveals that a large percentage of the total energy is concentrated in the low frequency range of the signal spectrum. This low frequency information is common to signals which are similar in form, while it is the higher frequency information which distinguishes similar signals. One would therefore expect that the selectivity of a matched filter can be improved by blocking transmission of light in the low frequency range.

Photographic film has been and continues to be a basic medium for recording data in optical processing and filtering systems. One method for realizing the bandlimited matched

filter, using the saturation characteristics of photographic film, is as follows. Overexposure by the signal light component during filter formation causes the film to saturate in the low frequency range since most of the energy is concentrated near the zero frequency. Simultaneously, the signal level is increased in the high frequency range and the signal to noise ratio of the higher frequency components is increased significantly. That is, the normally limited upper frequency cut off has been extended (7). The situation discussed here is illustrated in Figure 1, where films have been subjected to different exposures to record the Fourier spectrum of the signal (rectangular aperture).

From Figure 1, it can be seen that as the lower cut off frequency increases, the high frequency cut off increases and vice-versa. The upper cut off frequency can be determined by comparison of the noise level of the recording medium (film) and the apparent spectral width of the filter function.

In short, it can be said that the upper and lower cut off depends on the exposure time, developing time, type of film and signal to reference intensity ratio during exposure. It is the latter factor which is employed in practice. Also, in practice, the low frequency bandstop can be made to exhibit uniform opacity by use of an opaque mask, thus alleviating any gray area which might exist.

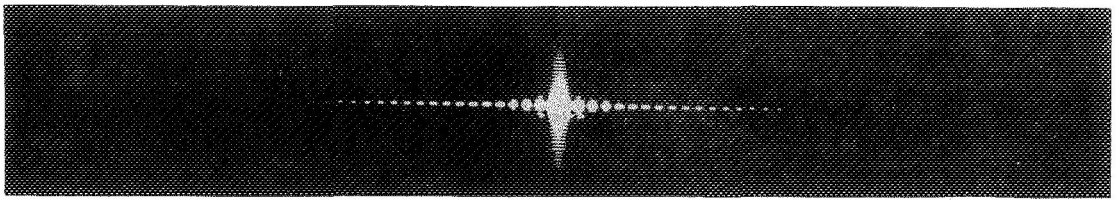

(a) Exposure $E_1$

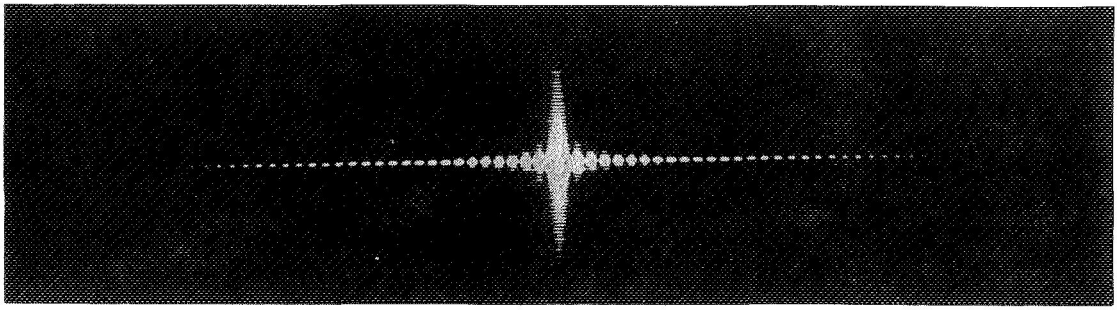

(b) Exposure $E_2 > E_1$

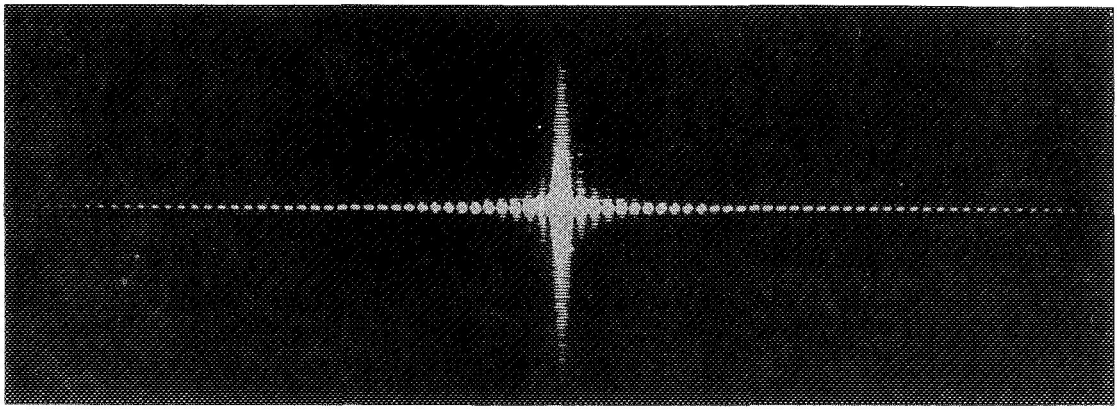

(c) Exposure $E_3 > E_2$

Figure 1. Fourier spectrum of a rectangular aperture, illustrating bandwidth variations as a function of exposure.

## Bandlimited Matched Filter Model

It has been intuitively reasoned in the previous section that the selectivity of a matched filter can be improved by use of a high pass filter in conjunction with a wideband matched filter. A related aspect is the expectation that such additional filtering will alter the output light distribution (i.e., the resulting correlation light intensity). Both of these considerations have been investigated theoretically by use of a bandlimited matched filter model. The idealized meteor trail model or rectangular aperture was used throughout this study as the input signal and the signal to which the filter is matched.

In general, the bandlimited matched filter model consists of a matched filter operating under band pass filter constraints. The bandpass filter can be considered as a combination of a low pass and a high pass spatial frequency filter. If an obstruction is located such that it prohibits light being transmitted in a region above a certain spatial frequency (i.e., the high frequency cut off), it is called a low pass filter. This type filter is shown in Figure 2(a). Otherwise, if an opaque obstruction is placed in the low frequency region (around the zero frequency component) of the two-dimensional frequency plane such that it prohibits light being transmitted through that portion of the plane which is below a certain spatial frequency (i.e., the low frequency cut off), it is called a high pass filter. Figure 2(b) depicts this situation.

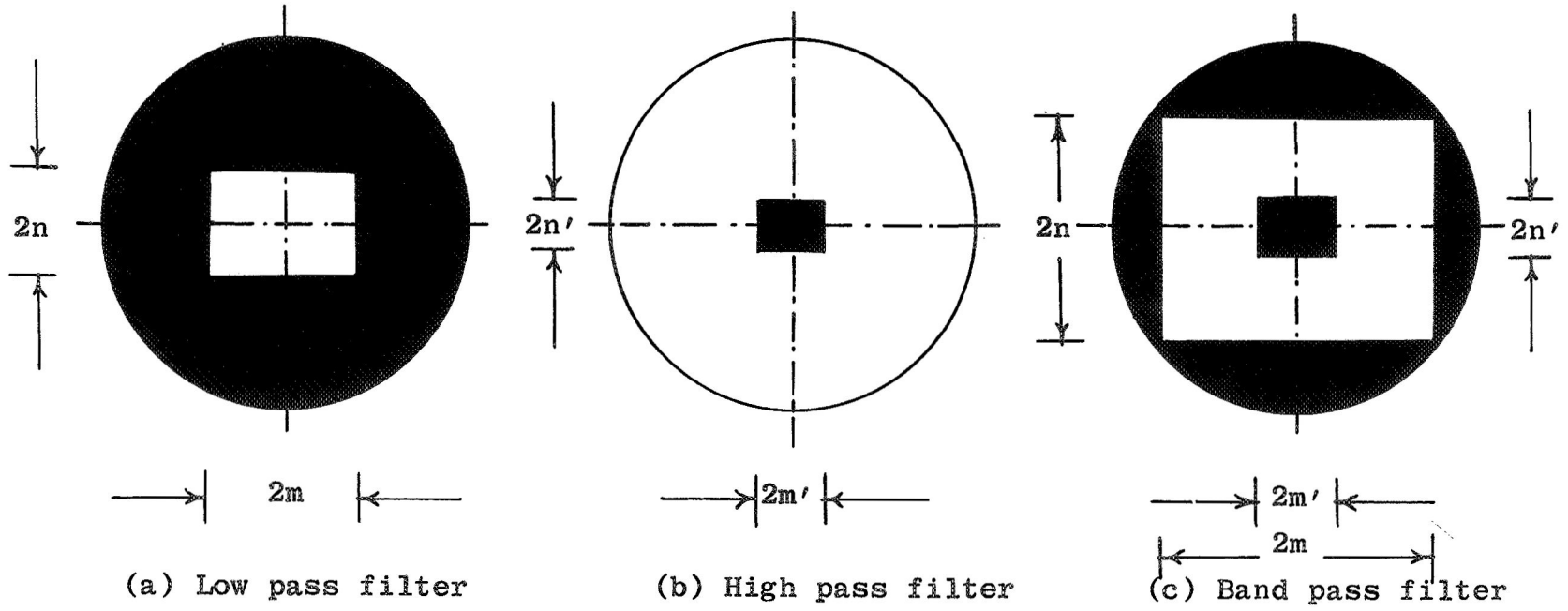


Figure 2. Models of spatial frequency filters.

Combining the characteristics of the high pass and low pass spatial frequency filters produces a band pass filter, as shown in Figure 2(c). This is an ideal band pass filter in that it exhibits infinite rejection above and below the respective cut off frequencies. In addition, the filter transfer function is entirely real. Thus, the band pass filter transfer function is given by

$$H_1\left[\frac{x_2}{\lambda f_1}, \frac{y_2}{\lambda f_1}\right] = \begin{cases} 1, & m' < \left|\frac{x_2}{\lambda f_1}\right| < m \text{ and } n' < \left|\frac{y_2}{\lambda f_1}\right| < n \\ 0, & \text{elsewhere} \end{cases}, \quad (1)$$

where $(m',n')$ and $(m,n)$ are respectively the lower and upper cut off frequencies, in two dimensions. Here $\lambda$ is the wavelength of the monochromatic light and $f_1$ is the focal length of the transform lens (see Appendix A). Contrasted with its electronic counterpart, the band pass filter described here is a realizable filter.

A matched filter may be described by the transfer function (2)

$$H_2\left[\frac{x_2}{\lambda f_1}, \frac{y_2}{\lambda f_1}\right] \propto \tilde{G}^*\left[\frac{x_2}{\lambda f_1}, \frac{y_2}{\lambda f_1}\right]. \quad (2)$$

Here, $\tilde{G}$ is the Fourier transform of $G(x_1,y_1)$, the signal to which the filter is matched.

Combining the transfer functions for the band pass filter and the matched filter yields the composite transfer function

$$H_1\left[\frac{x_2}{\lambda f_1}, \frac{y_2}{\lambda f_1}\right] = H_1\left[\frac{x_2}{\lambda f_1}, \frac{y_2}{\lambda f_1}\right] H_2\left[\frac{x_2}{\lambda f_1}, \frac{y_2}{\lambda f_1}\right]. \quad (3)$$

The above transfer function describes the bandlimited matched filter model.

Analysis of Bandlimited Matched Filters

The correlation related output (amplitude distribution) of a coherent optical matched filter system is given by Equation A-8 of Appendix A, where a general matched filter type optical correlator is described and analyzed. In terms of a two-dimensional Fourier transformation, the output can be written as

$$\Phi(x_3,y_3) \propto \int_{-\infty}^{\infty}\int_{-\infty}^{\infty} \tilde{S}(u,v)\, \tilde{G}^*(u,v) \exp\left[-2\pi i(x_3u + y_3v)\right]dudv, \quad (4)$$

where $(x_3,y_3)$ are the output plane variables and $(u,v)$ are the spatial frequency variables. The term in the argument of the complex exponential, $(-\alpha\lambda f)$, of Equation A-8 serves to translate the output off-axis, but in no way affects the amplitude or light distribution; thus, it will not be carried through the remainder of this report.

A filter which is matched to a rectangular aperture having dimensions as shown in Figure 3(a) was chosen for investigation of bandlimiting effects. That is,

$$G(x_1,y_1) = \text{rect}\left[\frac{x_1}{a'}\right] \text{rect}\left[\frac{y_1}{b'}\right] \quad (5)$$

and the two-dimensional Fourier transform is

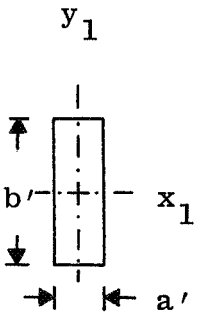


$a' = 1$ mm.*, $b' = 3$mm.*

(a) The signal to which the filter is matched.
(* dimensions used in experimental work)

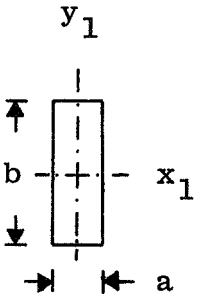


Case 1: $a'/a = 1$, $b'/b = 1$

Case 2: $a'/a = 2$, $b'/b = 1$

Case 3: $a'/a = 0.5$, $b'/b = 1$

(b) Input signal formats.

Figure 3. Signal formats used in theoretical and experimental matched filter model studies.

$$\tilde{G}(u,v) = a'b' \operatorname{sinc}(\pi a'u) \operatorname{sinc}(\pi b'v) \tag{6}$$

Here, $(x_1,y_1)$ are the input plane variables, and the apertures are assumed to be illuminated by light amplitude of unit value.

Three different input signals were chosen as shown in Figure 3(b). For the inputs,

$$S(x_1,y_1) = \operatorname{rect}\left[\frac{x_1}{a}\right] \operatorname{rect}\left[\frac{y_1}{b}\right] \tag{7}$$

and

$$\tilde{S}(u,v) = ab \operatorname{sinc}(\pi au) \operatorname{sinc}(\pi bv). \tag{8}$$

It should be noted here that according to the inputs selected, a correlation analysis will yield cross-correlation in the $x_3$ dimension and auto-correlation in the $y_3$ dimension.

A wideband filter (i.e., a matched filter with no bandlimiting) can be analyzed by direct use of the above output relation. For the bandlimited cases, the respective cut off frequencies are introduced into Equation 4 through the limits of integration as

$$\Phi(x_3,y_3) \propto 2 \int_{n'}^{n} \int_{m'}^{m} \tilde{S}(u,v) \tilde{G}^*(u,v) \exp[-2\pi i(x_3u + y_3v)]dudv. \tag{9}$$

The above expression can be evaluated for rectangular aperture signals as indicated in Appendix D. Use of Equation D-2 was made to calculate various output correlation distributions. The one-dimensional light intensity distribution for the wideband filter is shown in Figure 5, corresponding to $y_3 = 0$. It is seen in this figure that the peak auto-correlation intensity equals that for cross-correlation with a larger aperture. One-dimensional curves corresponding to $x_3 = 0$ would be similar to the auto-correlation curve except for a simple scale change.

Cut off frequencies for the bandlimited cases were estimated from several filters which were recorded for experimental purposes. A typical low pass case is shown in Figure 6. These curves demonstrate the fact that typical upper cut off frequencies are sufficiently high to be considered infinite, since the curves of Figure 6 are almost identical to those of the wideband filter shown in Figure 5. Therefore, the assumed bandlimited matched filter model can be considered to be simply a high pass filter model, at least in the absence of noise.

For the high pass filter case, correlation intensity curves are shown in Figure 7 and 8. The low frequency cut offs correspond to the first and third zeros respectively of the sinc function shown in Figure 4. In these

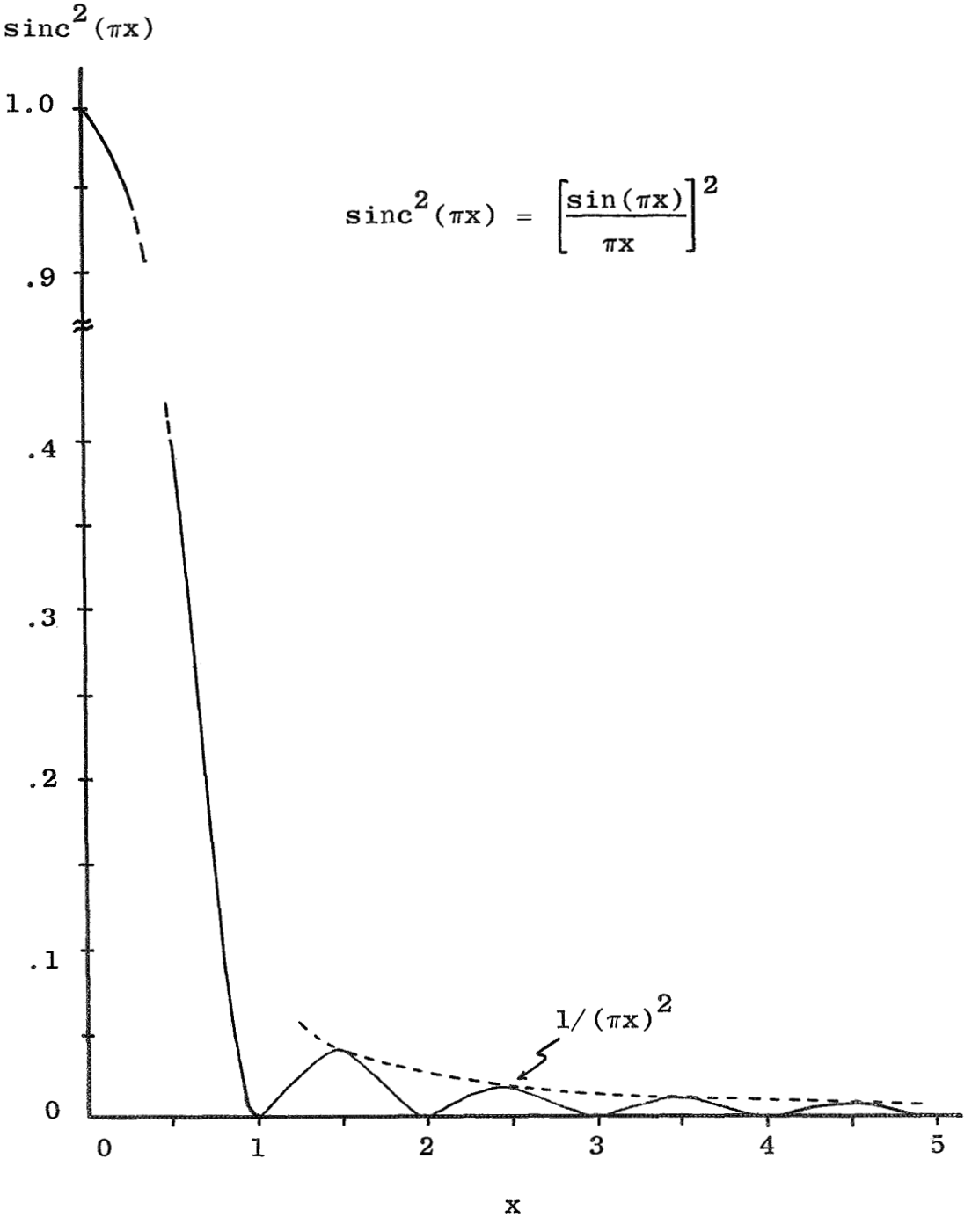


Figure 4. Plot of squared sinc function.

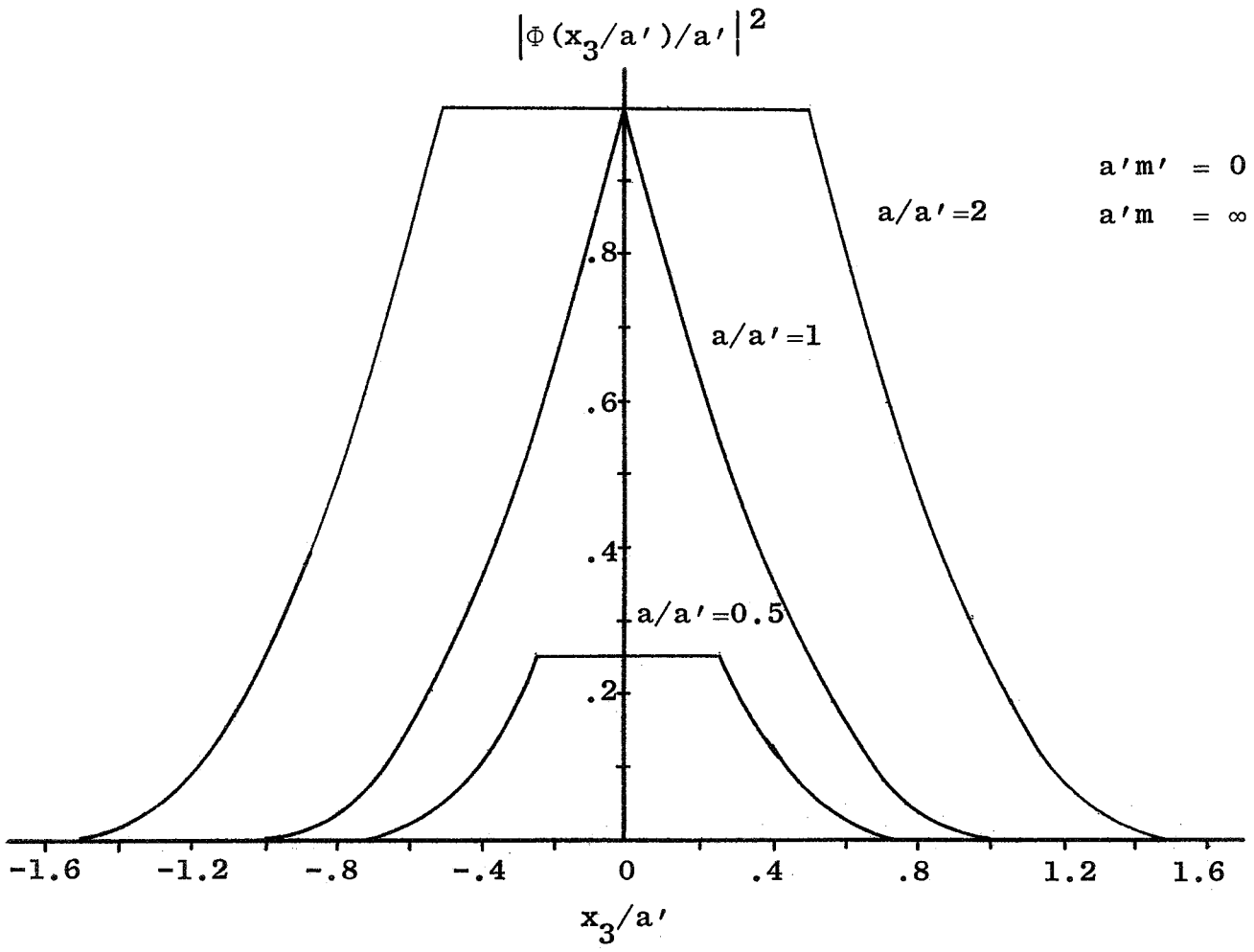


Figure 5. One-dimensional curves of wideband correlation intensities corresponding to rectangular aperture signal formats.

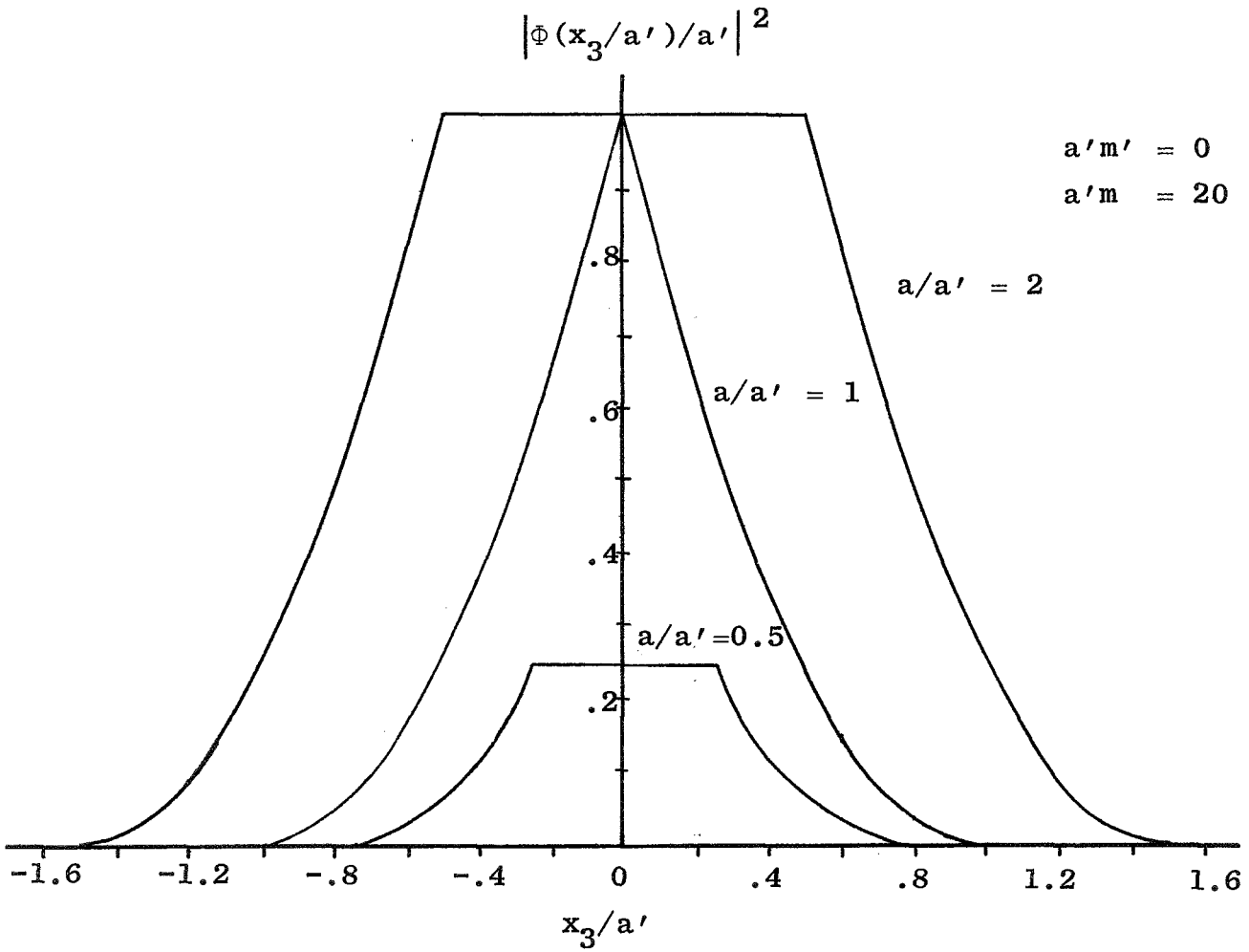


Figure 6. One-dimensional curves of low pass filtered correlation intensities corresponding to rectangular aperture signal formats.

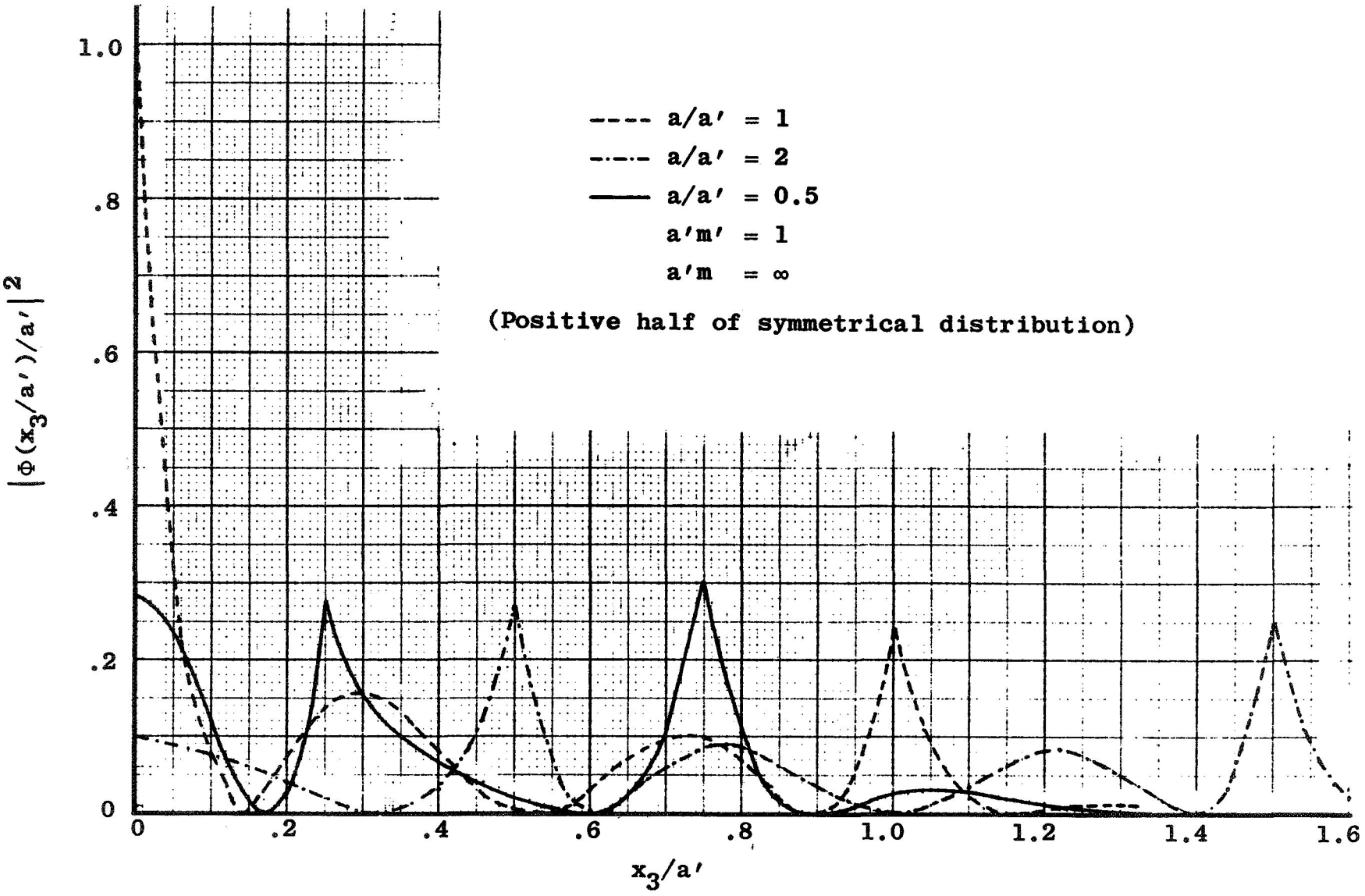


Figure 7. One-dimensional curves of high pass filtered correlation intensities corresponding to rectangular aperture signal formats.

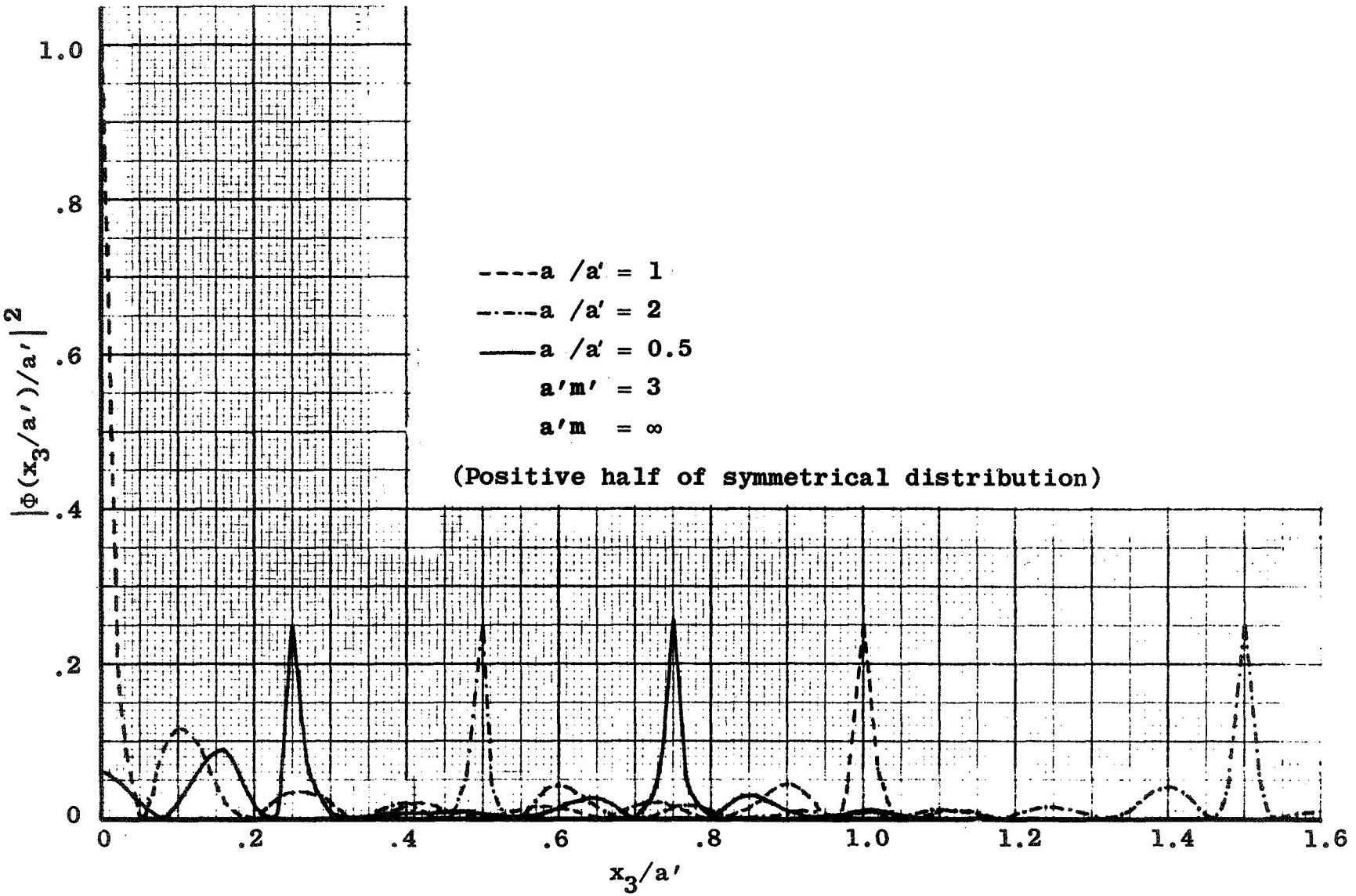


Figure 8. One-dimensional curves of high pass filtered correlation intensities corresponding to rectangular aperture signal formats.

figures, it is noted that the output light distribution is significantly altered as a result of bandlimiting. Especially notable is the fact that more than one "spot" of light may be observed in the output plane.

Concerning the filter selectivity as a function of bandlimiting, it is seen that the difference in the values of correlation intensities (measured along the ordinates of Figures 5, 7 and 8) between auto-correlation and cross-correlation increases as the lower cut off frequencies increase. A more complete set of data on filter selectivity is presented in Figure 9, normalized to unity to emphasize the relative selectivity of the filters. The selectivity curves in this figure were obtained from Equation D-2, representing a wideband filter and filters with low frequency cut offs corresponding to the first and third zeros of the sinc function shown in Figure 4. The general characteristics of the selectivity curves show that selectivity is improved as the lower cut off frequency increases; however, for the two bandlimited cases, the selectivity curves are not monotonically decreasing curves about the point $a/a' = 1$. These results indicate that the process employed here to enhance matched filter selectivity is not as straight forward as it initially appeared to be. An explanation of the radical behavior of the selectivity curves lies in the

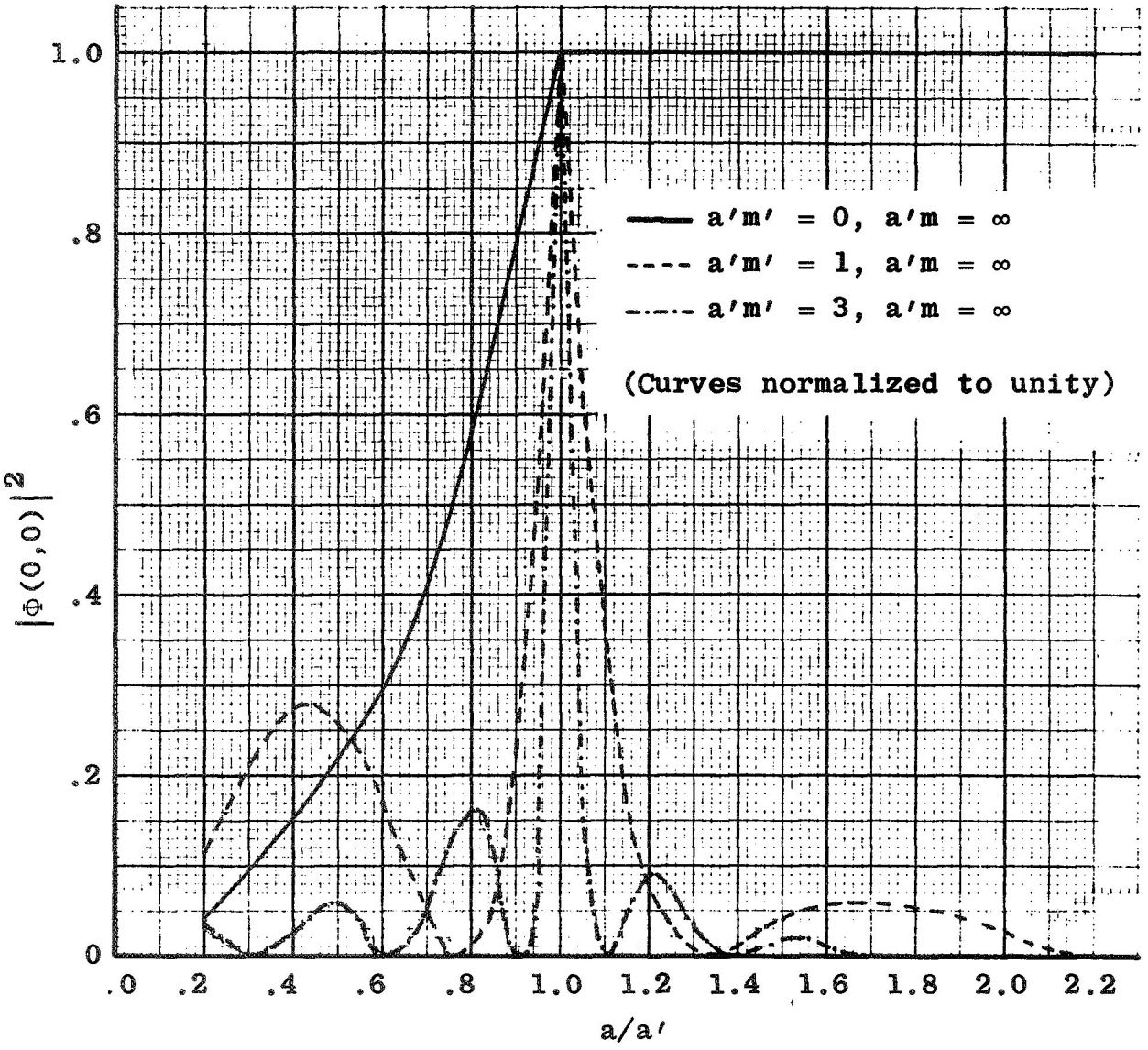


Figure 9. Bandlimited matched filter selectivity curves.

fact that correlation under high pass conditions actually consists of a comparison of the edges of the rectangular apertures involved. This is illustrated in Figure 10 where the reconstruction of a Fourier transform hologram (matched filter) is shown. The absence of low frequency information due to film saturation is noted here. Furthermore, the edges are not sharp as demonstrated in Figure 11 for a bandlimited straight edge (e.g., one side of a rectangular aperture). Thus, $|\Phi(0,0)|^2$ for crosscorrelation becomes a complex function of aperture dimensions and cut off frequency, as predicted by Equations D-2 and D-3.

Experimental Investigation of Bandlimited Matched Filters

The analytical results of the previous section show that matched filter operation is a function of its bandpass characteristics. It was shown that the output light distribution is significantly altered as a result of bandlimiting, while filter selectivity generally improves as the lower cut off frequency is increased. It was assumed that the upper cut off frequency is typically high enough to be considered infinite. Further, it was observed that little change takes place in the light distributions for normalized lower cut off frequencies greater than unity. To lend support to the theoretical results, several experiments were carried out to determine the effects of bandlimiting upon matched filter operation.

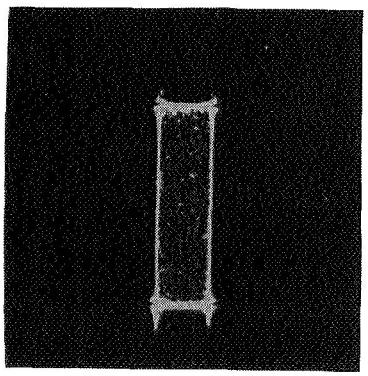

Figure 10. Reconstruction of a bandlimited matched filter.

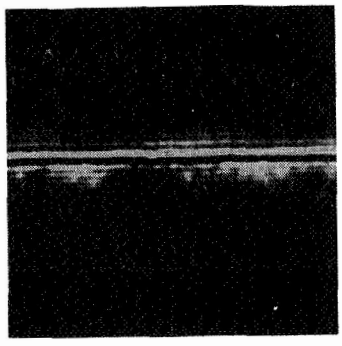

Figure 11. Bandlimited image of a straight edge.

The general steps carried out in the filter formation and correlation processes were similar to those discussed in Appendix A. The exception to this statement is that the signal light component was made sufficiently large to overexpose the film (matched filter recording medium) in the low frequency region; thus, the resulting matched filter was a high pass device. Aspects of film exposure and processing will be discussed in Chapter III, where it will be shown that a signal to reference component ratio, S/R, equal to or greater than approximately 1.6 can cause film saturation. Experimental results of bandlimiting are illustrated in Figure 12. The filter from which these data were obtained was a high S/R filter, with an estimated lower cut off frequency corresponding to the first zero of the sinc function of Figure 4. Multiple "spots" are seen to appear in each distribution of Figure 12, as the theory predicts. These points of high intensity are very useful when qualitative results are desired (see Figures 7 and 8).

A closed circuit TV system, as described in Appendix C, was also used to obtain intensity recordings for correlation outputs. The TV camera was placed such that the photosensitive area of the Vidicon was located in the output plane. A single line scan, passing through the center of the output light distribution, was observed via an oscilloscope. Figure 13 illustrates this type of visual readout. The two traces in this figure correspond to the autocorrelation and a crosscorrelation

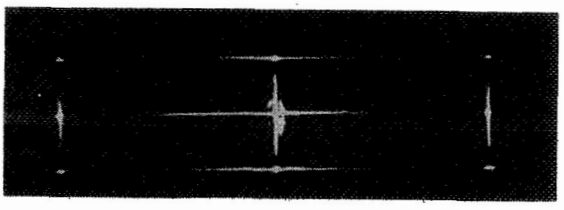

(a) Autocorrelation with a=1mm; b=3mm

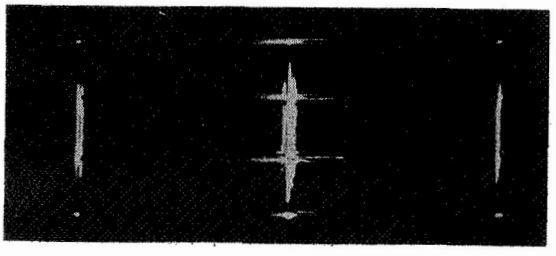

(b) Crosscorrelation with a=2mm; b=3mm

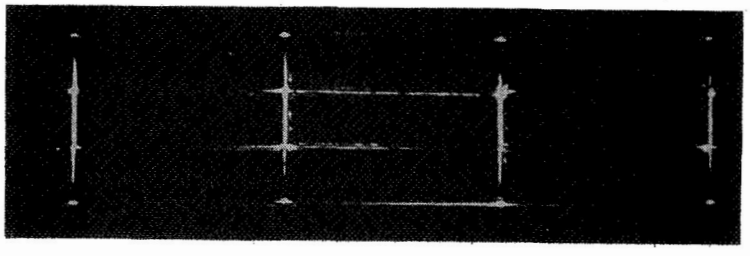

(c) Crosscorrelation with a=2mm; b=6mm

(d) Crosscorrelation with a=0.5mm; b=3mm

Figure 12. Bandlimited correlation intensity distribution.

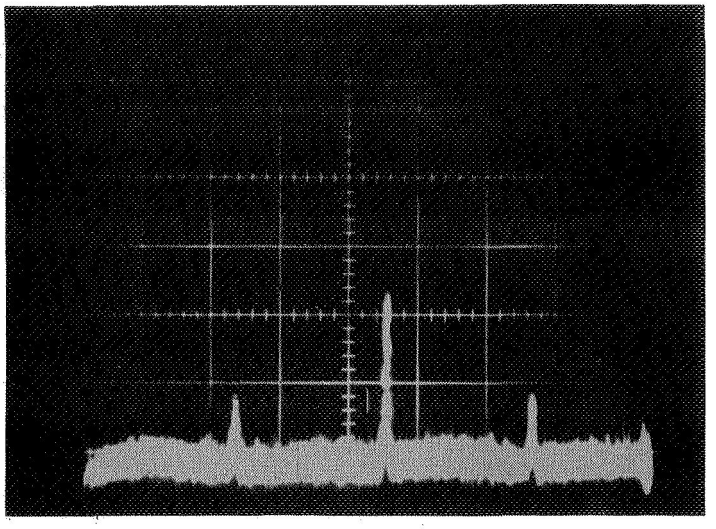

(a) Autocorrelation with a=1mm; b=3mm

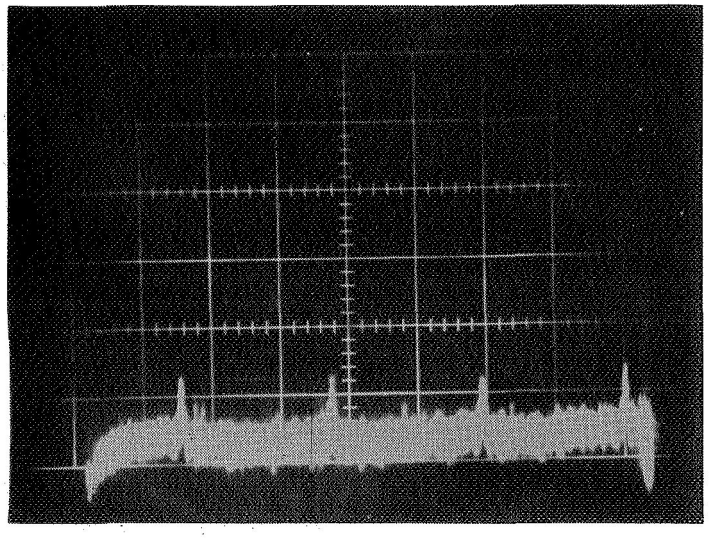

(b) Crosscorrelation with a=2mm; b=6mm

Figure 13. Traces of bandlimited correlation intensity distributions.

of Figure 12. Comparison of the relative intensities of these two traces with the theoretical data shows good agreement.

An experiment was conducted in an effort to lend support to the matched filter selectivity characteristics which the filter model predicts. However, it is difficult to obtain a prescribed lower cut off frequency experimentally, primarily due to the fact that the lower cut off frequency is not well defined. An approximate relation between cut off and S/R is developed in the next chapter. Nevertheless, desired values of cut-off can be approximated. Selectivity data were obtained via the TV line scanner for filters made with a wide range of S/R values. These data are presented in Figure 14.

Experimental results obtained in the study of band-limited matched filter operation is in general agreement with the theory. Theory and experiment indicate little change in filter operation when the lower cut off frequency exceeds the normalized value of unity. The bandlimited output light distributions contain "spots" of light which are useful in attempts to characterize an unknown signal. In addition, bandlimiting can be employed to improve filter selectivity when needed.

Although the results obtained in the study of the operation of the matched filter as a function of its band-

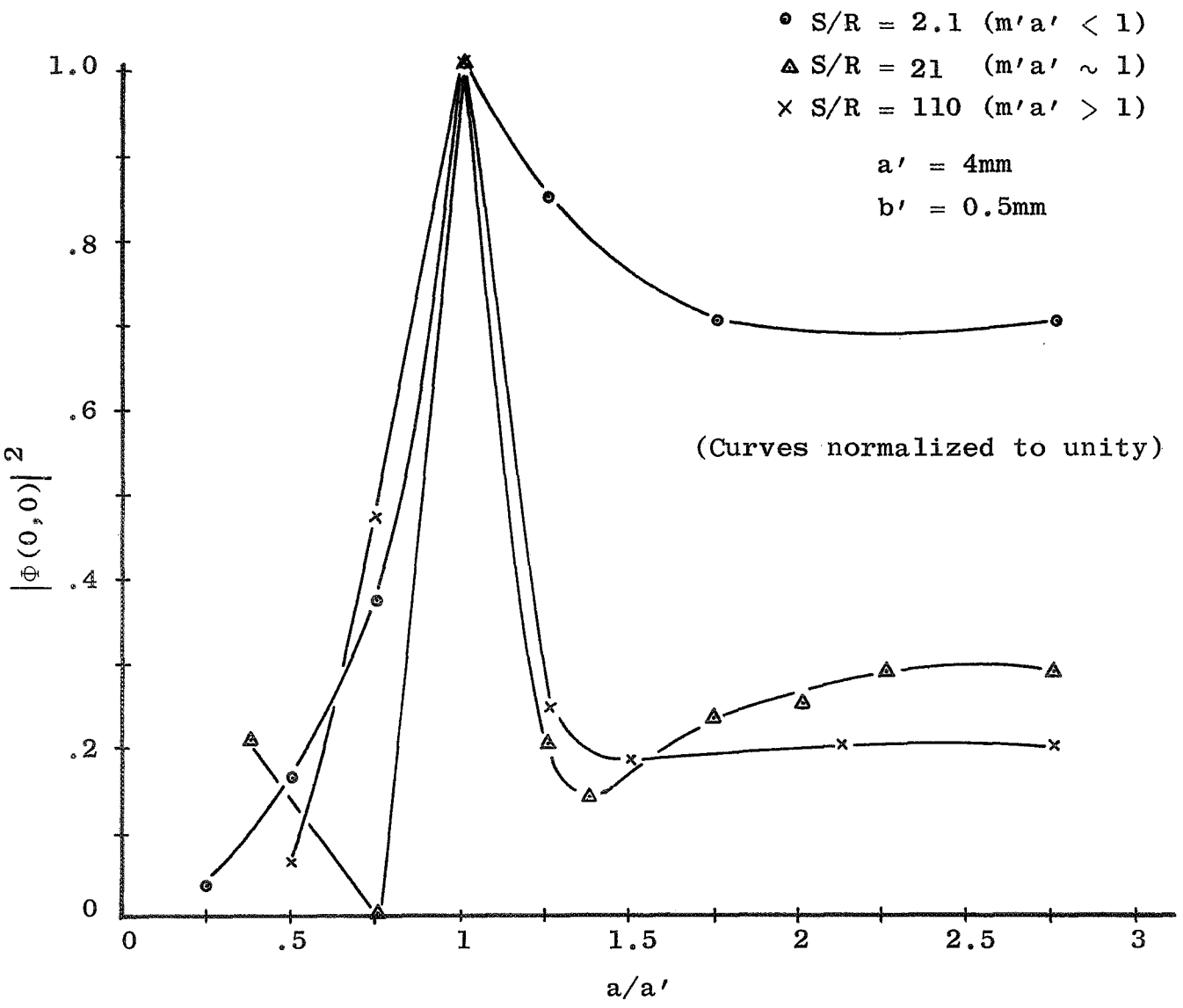


Figure 14. Experimental matched filter selectivity curves.

pass characteristics are peculiar to rectangular aperture type signal formats, several general conclusions may be drawn. The output correlation light distributions are significantly altered by bandlimiting, and the selectivity of matched filters can be improved by means of high pass filtering. Both of these effects are directly attributed to the fact that correlation is taking place between the respective aperture edges as opposed to the total aperture areas. Finally, it should be pointed out that selectivity desired for a particular application is a function of the objectives of that application.

# CHAPTER III

## SOME ASPECTS OF FILM CHARACTERISTICS AND PROCESSING RELEVANT TO MATCHED FILTER OPERATION

A discussion of matched filter operation as a function of its handpass characteristics was presented in the previous chapter. In this chapter, photographic film (the medium upon which the matched filter is recorded) characteristics are considered, and the non-linear effects of the film as they relate to the lower spatial frequency cut off of band-limited matched filters are discussed. In addition, matched filter diffraction efficiency is considered. Experimental results of several bleached filter experiments are presented.

### Film Characteristics

Several photographic films have been popular candidates as recording media for holograms and matched filters. The Agfa-Gevaert 8E and 10E series films offer high sensitivity around 0.6 microns with resolution in excess of 2000 lines/mm (8). These emulsions exhibit essentially a constant gamma ($\gamma = 4.3$). Presently, 8E75 and 10E75 are available. Another film type often employed is Kodak 649F spectroscopic film. This film offers resolution in excess of 3000 lines/mm, but its sensitivity is less than the Agfa-Gevaert types. Kodak 649F has an approximate gamma range of 1 to 3 for development times of 2 to 10 minutes in Kodak D-19 developer (9).

The experiments reported here were carried out using Kodak 649F photographic plates. This particular film was selected because its emulsion thickness of approximately 16 microns is desired for bleaching, contrasted with the less thick emulsion of the Agfa-Gevaert type films. One method of presenting film characteristics is by way of an amplitude versus exposure curve. Such a curve is shown in Figure 15 (10). The data for this curve were obtained by exposing the film through step density wedges with a He-Ne laser. The film was developed in Kodak D-19 developer for three minutes at 76°F, stopped for 30 seconds, fixed for three minutes and washed for 30 minutes. Figure 15 shows that the maximum linear dynamic range of the film is achieved when operating about an amplitude transmission of 0.5.

A number of matched filters were exposed for varying times to determine the optimum density range with respect to filter diffraction efficiency. After exposure, the plates were developed according to the procedure described above. The various filters were compared by measuring their diffraction efficiency via a photomultiplier tube. Diffraction efficiency is defined here as the ratio of the total intensity in the output correlation component to the total intensity of the light incident upon the filter. Typical data obtained in this experiment is shown in Figure 16, where diffraction efficiency is plotted versus density. The density values were obtained by measuring the density due to reference beam exposure only. This density value was used because the

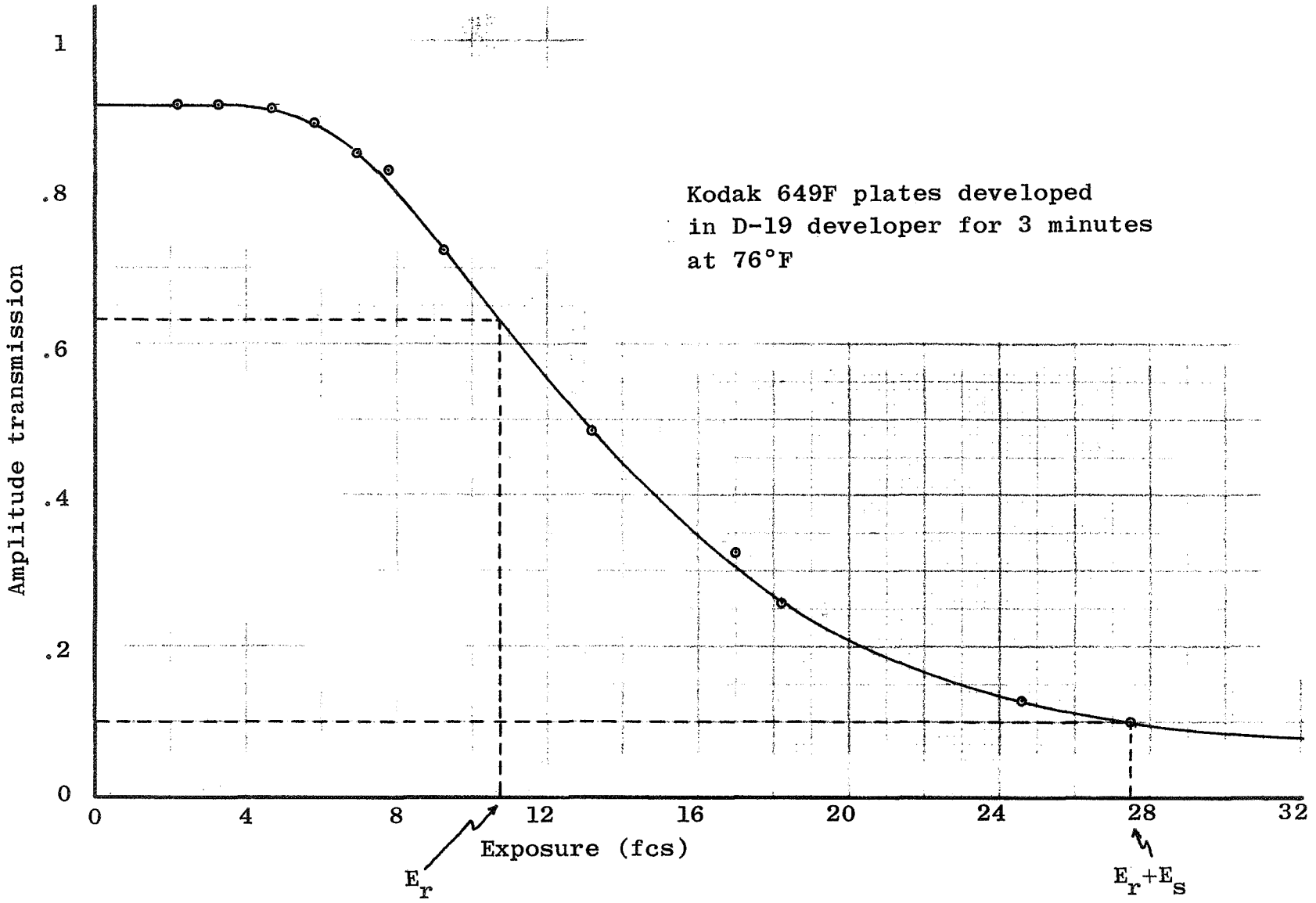


Figure 15. Amplitude transmission versus exposure curve.

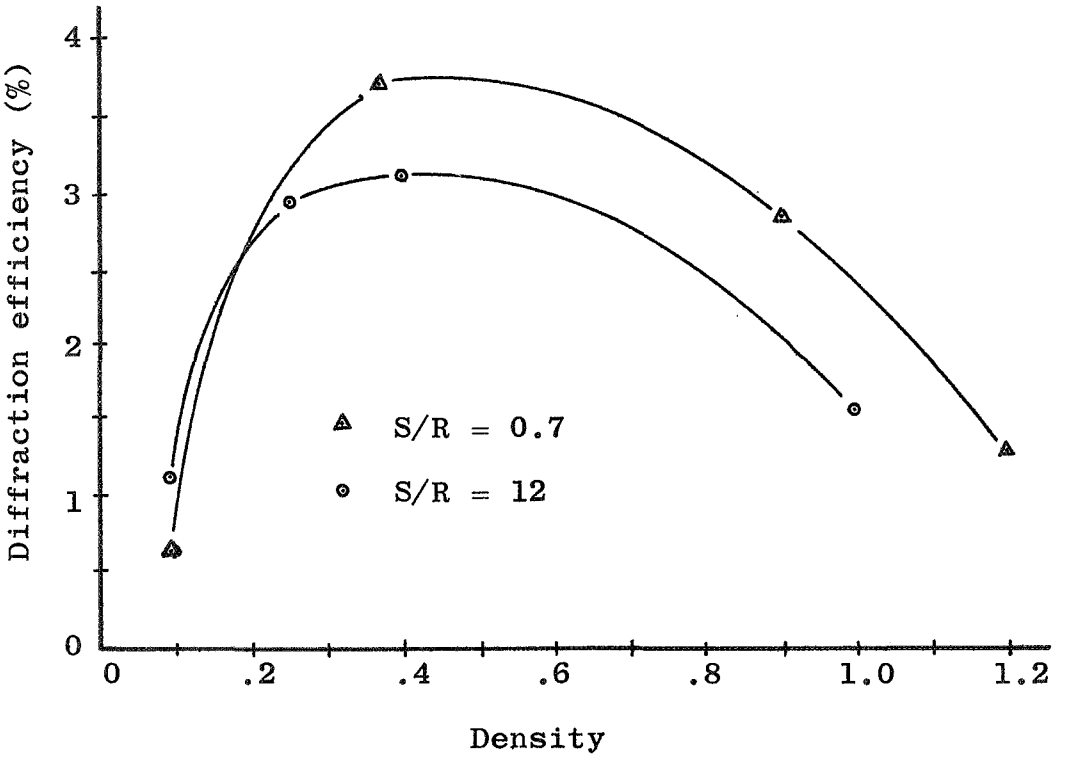


Figure 16. Diffraction efficiency as a function of density.

density resulting from exposure by the reference and signal beam varies across the filter, as a function of the signal spectrum. It was, therefore, necessary to relate the components of signal and reference intensities by a signal to reference intensity ratio, S/R. A series of filters were made with several values of S/R and it was found that the density range of maximum diffraction efficiency was 0.3 to 0.5 for each ratio. A plot of diffraction efficiency versus S/R is shown in Figure 17. It is noted here that the efficiency is reduced as S/R increases. This is due to the fact that higher ratio filters are saturated in the low frequency region of the filter where most of the signal energy is concentrated; thus, much of the light is blocked in the higher S/R filters. The higher S/R filters are non-linear and it was found that they produced higher order output images. These were determined to contain up to 15% of the energy of the first diffracted order (i.e., correlation output component) for filters with S/R on the order of 100.

Bleached Matched Filter Experiments

Since the matched filter is actually a Fourier transform hologram, the bleaching process which has been applied to holograms was considered. A brief discussion of bleaching theory is presented in Appendix E, along with several formulae for chemical bleaches. The bleach used in this work was the

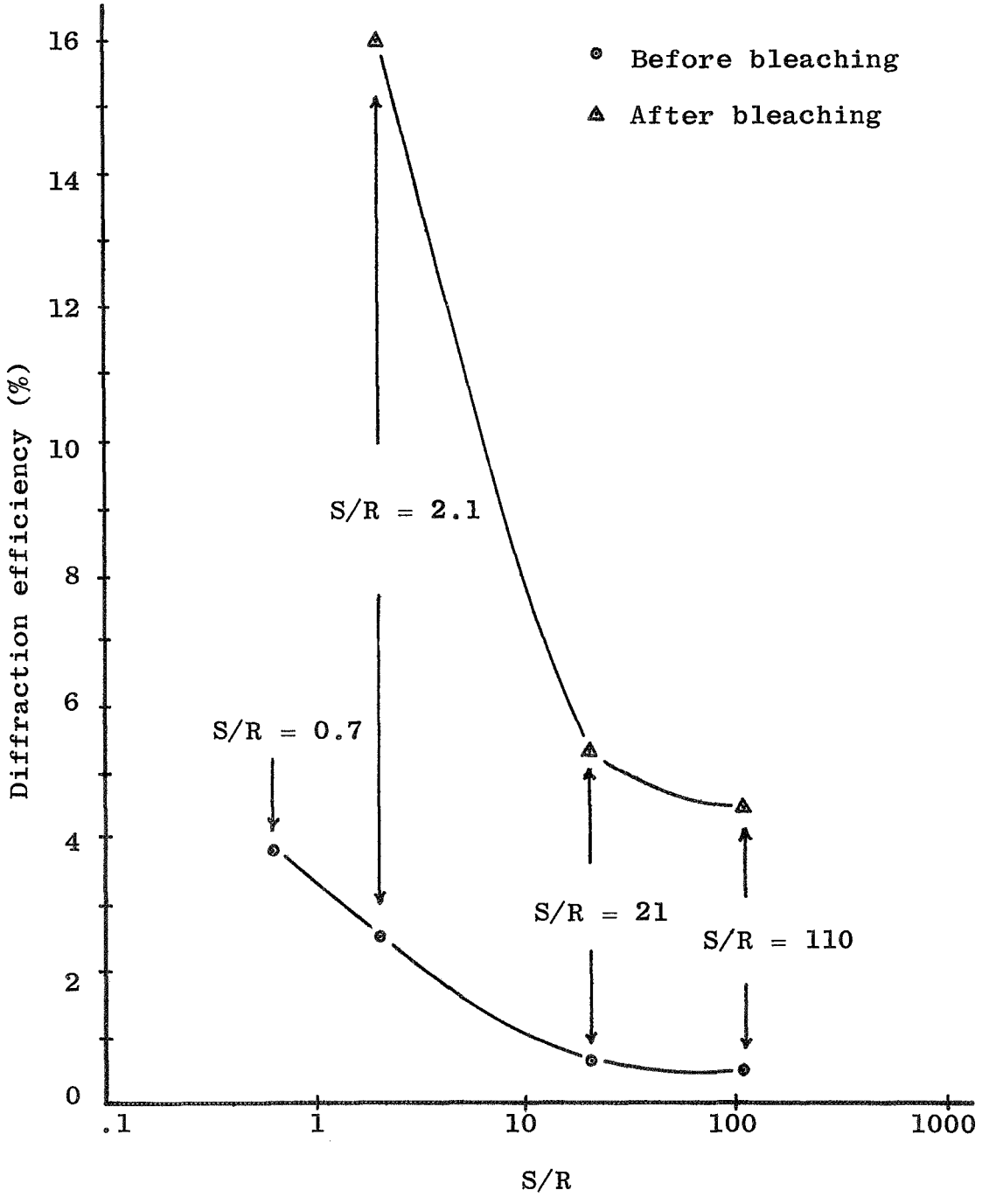


Figure 17. Diffraction efficiency as a function of S/R.

potassium ferricyanide type discussed in Appendix E. Specifically, the bleach was composed of eight grams of potassium ferricyanide and seven grams of potassium bromide to one liter of distilled water.

A series of matched filters were made with densities (due to reference beam exposure only) of approximately 0.4. The diffraction efficiencies were measured, each filter was bleached and the efficiencies were again measured. It was found that the apparent optimum bleaching time was dependent upon the S/R. Excessive bleaching of low S/R filters, for example, caused the filter performance to deteriorate. In such cases, the selectivity curve was found to increase with increasing values of $a'/a$, making the filter less useful for pattern recognition purposes. It is interesting to note here that the model analysis predicts this type result for $a'm' = 0$ and $am < 1$.

The results of bleaching the higher S/R filters showed an improved efficiency, depending upon the bleaching time. A plot of diffraction efficiency for unbleached and bleached filters is shown in Figure 17. Each filter here was bleached for 10 minutes, washed for 30 minutes, rinsed in Kodak Photo-Flo for 30 seconds and allowed to dry at least two hours in a laboratory environment. The S/R = 0.7 filter was ruined as a result of excessive bleaching, while the bleached S/R = 2.1

filter yielded a high efficiency but its selectivity deteriorated to a point where it was no longer useful for pattern recognition purposes. The greatest improvement was noted for the S/R = 21 and 110 filters, where the efficiencies are seen to be increased by a factor of about 7. The selectivity of these two filters tended towards that of a wideband filter, but maintained a high degree of selectivity. Figure 18 illustrates cross-sectional autocorrelation traces before and after bleaching.

From the foregoing discussion, it is apparent that bleaching must be carried out on a trial and error basis in order to obtain improved efficiency while maintaining sufficient selectivity for a particular application. It is apparent that a bleached filter exhibits bandpass characteristics which are a function of the S/R value and the bleaching time. In order to maintain some degree of selectivity, the filter should not be bleached until it is completely transparent. Practical use of bleached filters appears feasible when inadequate laser power is available. Otherwise, the problems associated with achieving optimally bleached filters probably do not warrant the use of such.

Relationship of the Lower Cut Off Frequency to S/R

Returning attention to the amplitude transmission versus exposure curve of Figure 15, an approximate relation between the lower cut off frequency of bandlimited filters and S/R

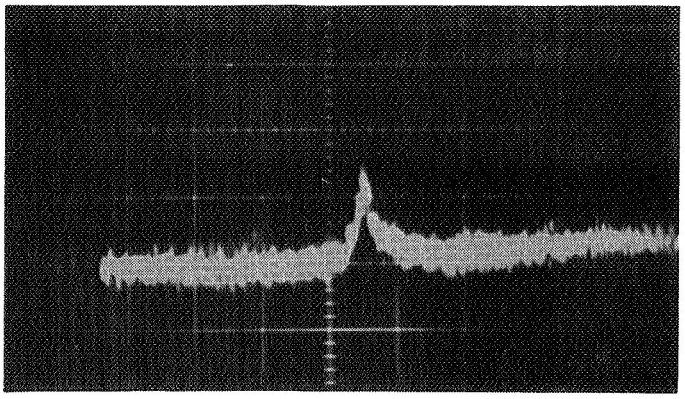

Unbleached (Vertical - 0.1 volts/div.)

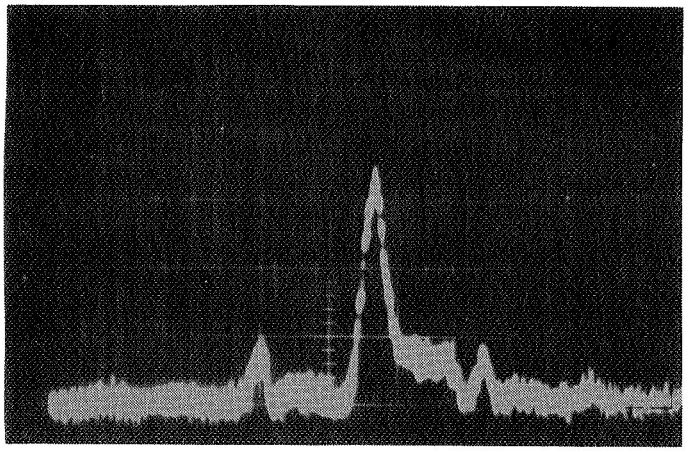

Bleached (Vertical - 0.2 volts/div.)

Figure 18. Illustrative traces of autocorrelation intensities before and after bleaching.

can be obtained. The cut off frequency is the most useful concept in theoretical considerations, where the S/R is a quantity which is easily measured in the laboratory. The ease with which cut off can be measured (e.g., via microdensitometer) depends on the geometry of the spectrum.

Assuming a matched filter recorded with a density (due to reference beam exposure only) of 0.4, it can be seen from Figure 15 that a S/R of approximately 1.6 will yield an amplitude transmission of approximately 0.1. Defining this value of amplitude transmission as the point where cut off occurs, an approximate relation between low frequency cut off and S/R may be given as

$$\left.\frac{S\ \mathrm{sinc}^2(\pi a' u)\mathrm{sinc}^2(\pi b' v)}{R}\right|_{\substack{u = m' \\ v = n'}} \simeq 1.6 \ .$$

In this expression $S = (Aa'b')^2$, where A is the amplitude of light incident upon the input plane during filter formation. The values of u and v which satisfy the above expression are then the lower cutoff frequencies. It should be emphasized that this relation is only a first order aproximation in that it neglects the effects of amplitude modulation of the average density of the recorded filter. In addition to the film transmission-exposure characteristics, film resolution and recording geometry (i.e., fringe frequency) are also factors in determination of the low frequency cutoff due to exposure "spillover" between the high density peaks of the matched filter fringes.

# CHAPTER IV

## APPLICATION OF MATCHED FILTER DETECTION TO METEOR TRAILS

The foregoing chapters have been concerned with characterization and operation of coherent optical matched filters. In this chapter, attention is restricted to specific application of matched filter systems for meteor trail detection. Consideration is given here to rotational sensitivity of matched filters employed for meteor trail detection and also signal contrast requirements for matched filter input data. Finally, results are presented which are representative of the ability of a matched filter to discriminate between meteor trails and stars.

### Rotational Sensitivity of Matched Filters

A matched filter is a space invariant filter. That is, within the limitations imposed by the transform lenses, translation of the input signal yields translation of the corresponding output by an amount proportional to that of the input signal. However, the orientation of the input signal is generally critical. The filter is matched to a particular signal having a particular orientation.

An experiment was conducted using ideal meteor trail models to determine the rotational sensitivity of matched

filters as a function of S/R. Two filters were employed, having S/R values of approximately 0.5 and 5. In each case, the signal to which the filter was matched was placed in the input plane and rotated while measuring the peak value of the correlation intensity, $|\Phi(0,0)|^2$, with the television line scanner. These data are shown in Figure 19. This figure shows that the higher S/R filter is more sensitive to rotation of the input signal (0.5 mm x 6mm rectangular aperture) than the low ratio filter. The effect of rotation in the input plane (and in the filter plane) is to smear the output light distribution, thereby decreasing the peak output intensity.

Effects of Input Signal Contrast on Matched Filter Operation

One of the most important factors affecting the operation of matched filter systems is that of the contrast between the input signal and the signal background. Here contrast is defined as the ratio of the light intensity transmitted by the signal (rectangular aperture) to that transmitted by the background. The effect of signal contrast is to alter the output peak correlation intensity, the detectable output quantity; and in addition, the light transmitted by the input signal background is partially diffracted into the background of the output plane. Thus, an output contrast can be defined as the ratio of the peak correlation intensity to the average intensity of the output background light. Figure 20 illustrates the

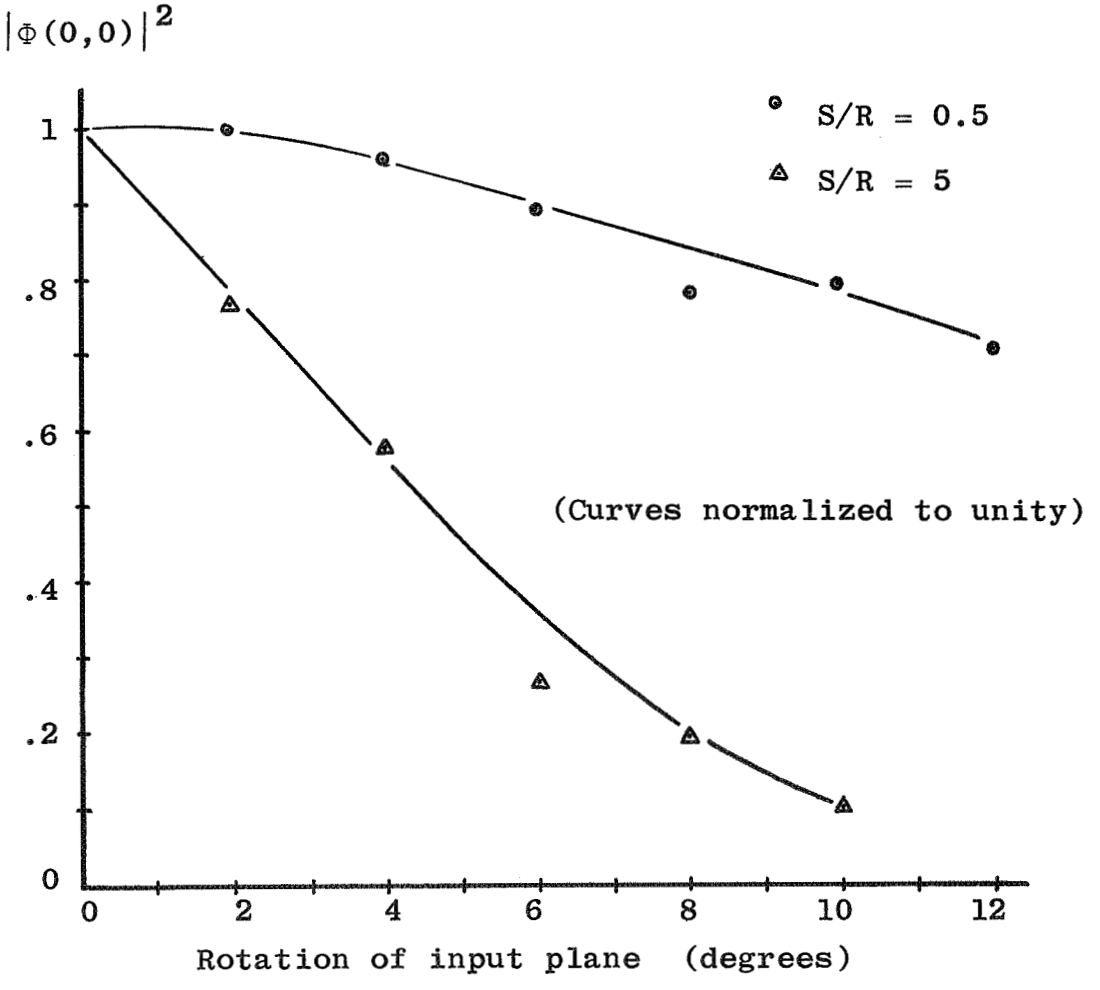


Figure 19. Effects of input plane rotation upon output autocorrelation intensity.

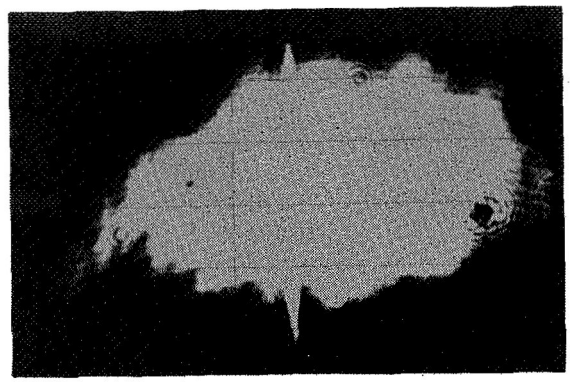

(a) Output with high transmission background in input plane, X4 magnification.

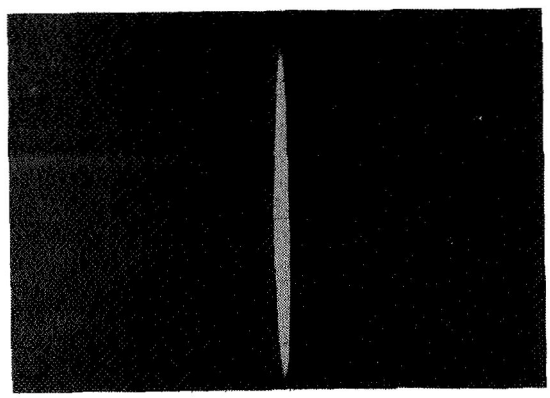

(b) Output with low transmission background in input plane, X4 magnification.

Figure 20. Illustration of input plane background transmission effects upon output light distribution.

correlation output corresponding to a very high input contrast as compared to an output corresponding to a low contrast input (one whose background is not opaque). The correlation intensity distributions in this figure are for rectangular aperture input signals and a matched filter made with a signal to reference ratio of approximately 0.5.

A set of fixed dimension rectangular aperture input signals ($a = a' = 0.5$mm, $b = b' = 6$mm) were recorded on photographic plates with varying contrasts. These signals were then applied to a matched filter and the outputs were measured. Two cases were considered. First the input background density was varied while the aperture area was made nearly transparent. These data appear in Figure 21, indicating detectable outputs for input contrast values of approximately 2 (see Figure 20). The second case consisted of a fixed input background density ($D \simeq 2$), and the aperture densities were varied. The data resulting from this experiment are presented in Figure 22, where it is seen that the peak correlation intensity varies in proportion to the transmission of the input apertures. It should be pointed out here that the minimum detectable output is a function of input and system introduced noise.

Star Pattern Rejection

Until this point, much has been said concerning matched filter selectivity or the ability of a filter to discriminate between similar signals. This is the most severe test of a

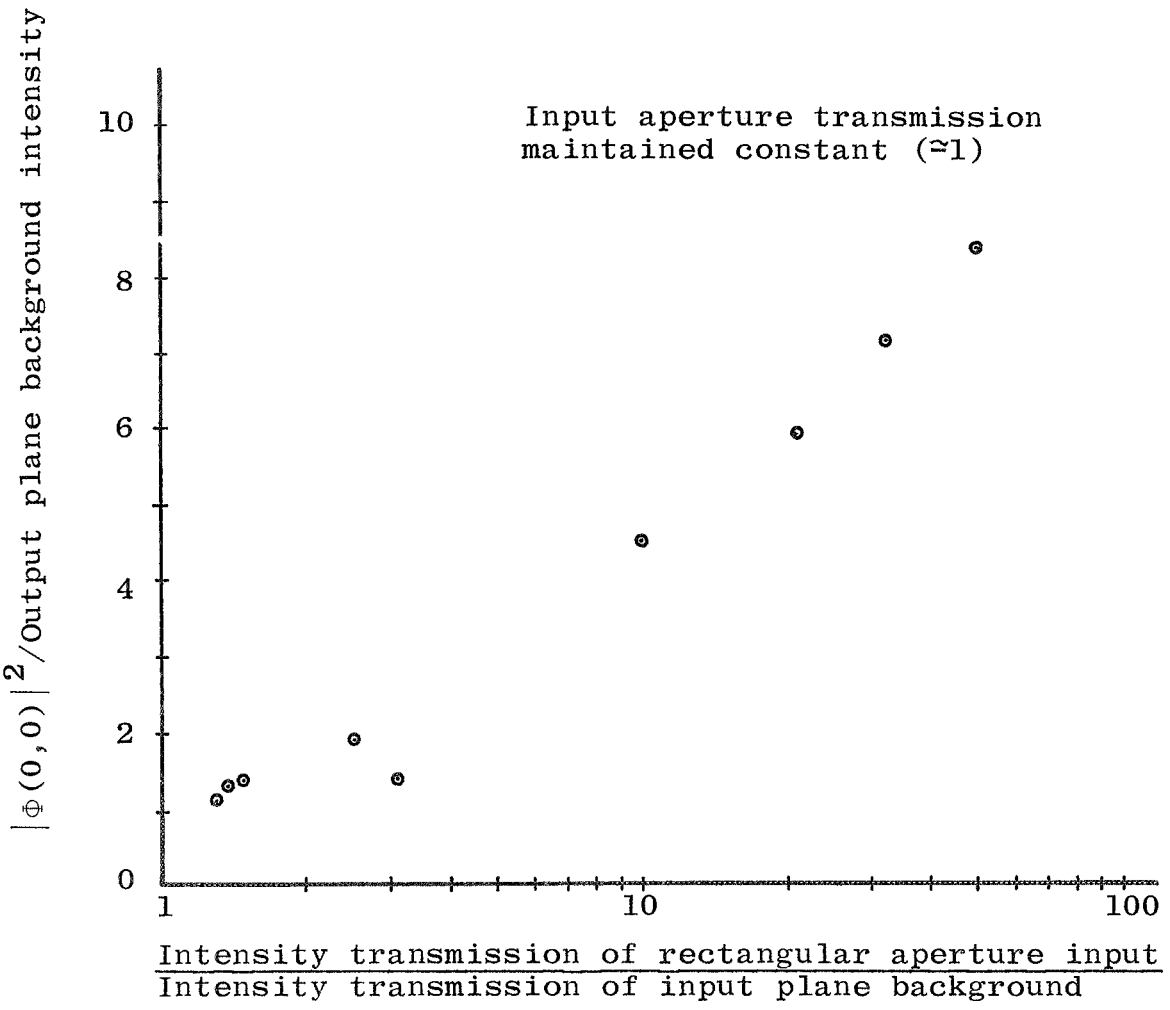


Figure 21. Output plane contrast as a function of input plane contrast.

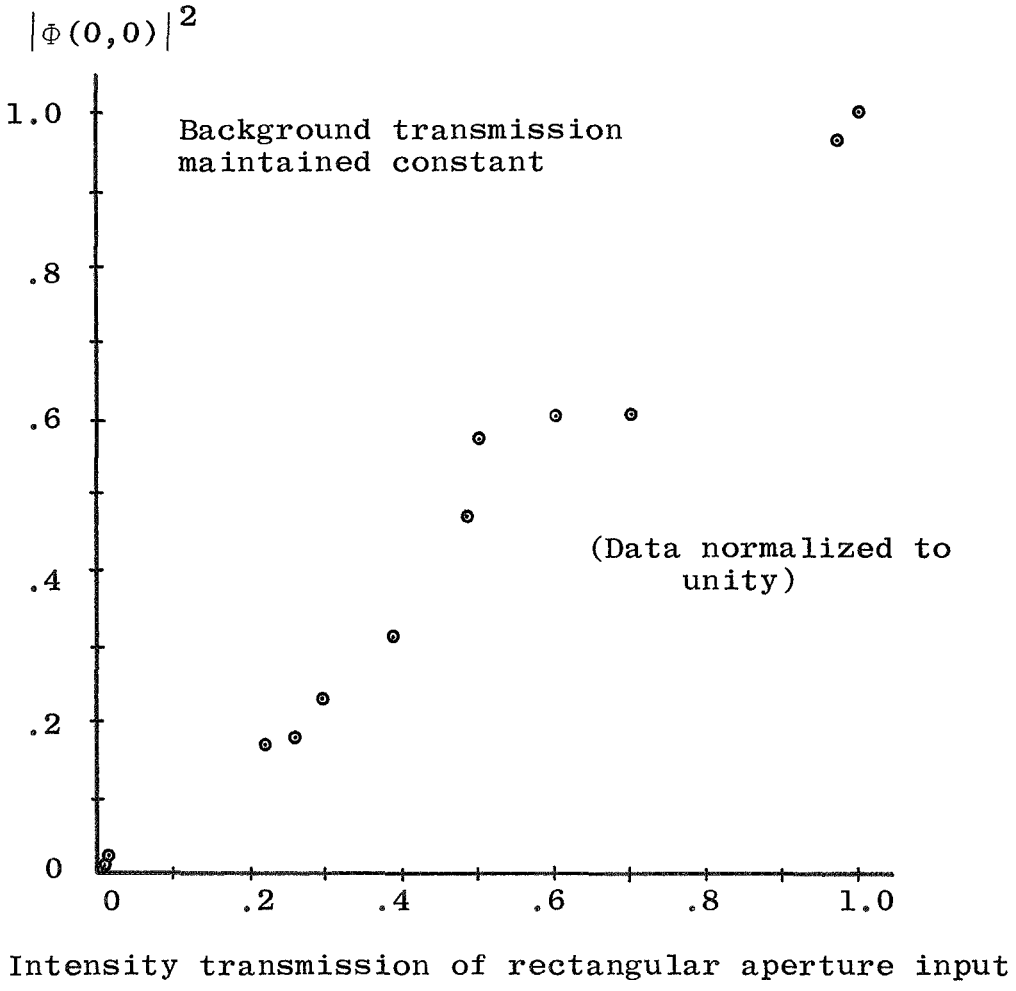


Figure 22. Output correlation intensity as a function of input rectangular aperture transmission.

matched filter. In the case where star patterns (modelled here by a circular aperture) are compared in a correlation analysis with meteor trails (rectangular aperture), very little similarity exists. The star images (i.e., the star images as they appear on film) may vary from tiny specks to light distributions which are relatively much larger. An example of a photograph of a night sky is shown in Figure 23, illustrating the variation in the sizes of stars as seen by an optical data processor. Dimensions of typical meteor trails would appear to the data processor as having widths of the order of star diameters, but the meteor trail lengths would appear relatively long compared with star diameters. Hence, because the two signal formats are dissimilar, a matched filter should provide a high degree of discrimination between the two.

The worse case with regard to detection of meteor trails from a star background is when large star patterns exist. Figure 24 illustrates a rectangular aperture autocorrelation and a rectangular aperture crosscorrelated with a circular aperture. These results show that the two light distributions are easily discernible. The effect of varying the size of the circular aperture is illustrated in Figure 25, which verifies that the larger star patterns, having the greater energies associated with them, produce the larger output intensities.

The results presented here are believed to be representative of the practical problem associated with meteor trail

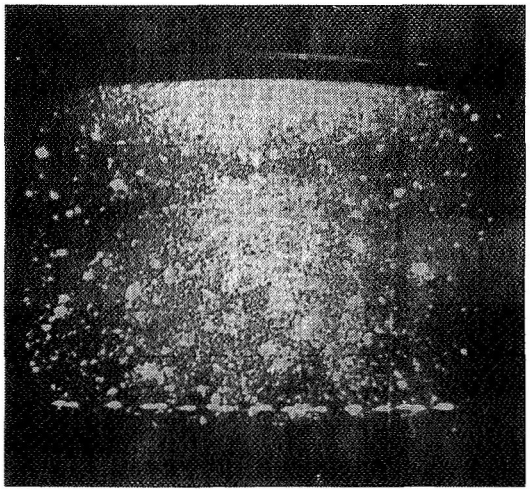

Figure 23. Illustration of star patterns.

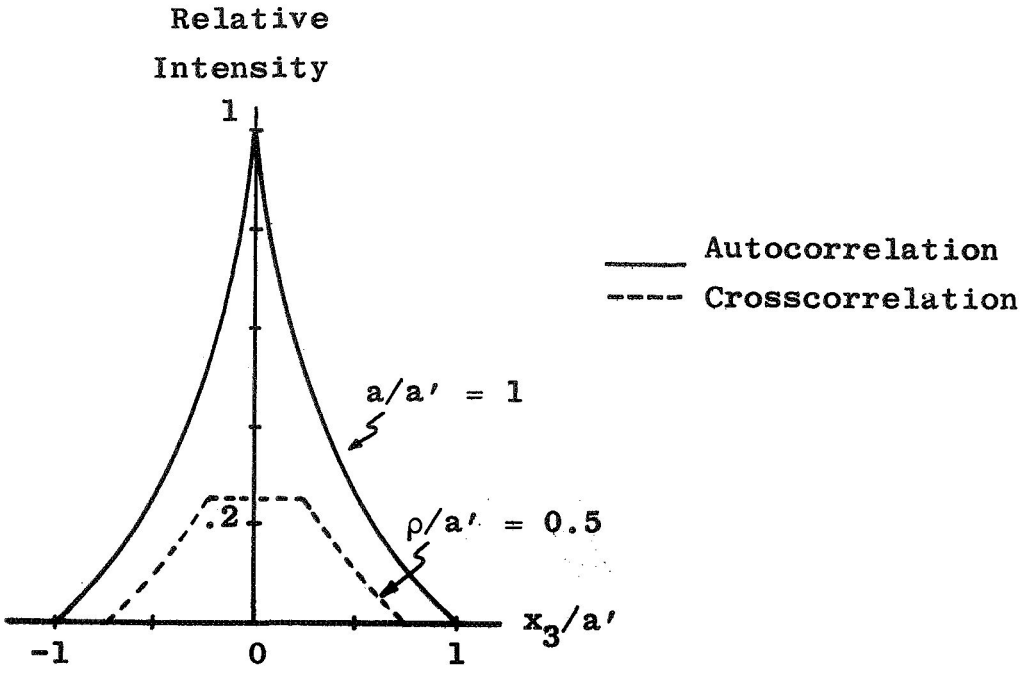


(a) Theoretical curves of rectangular aperture autocorrelation and crosscorrelation between a rectangular and circular aperture of diameter $\rho$.

(b) Experimental autocorrelation (right) and crosscorrelation (left), $a'$ = 4mm, $b'$ = 0.5mm and $\rho$ = 2mm, X4 magnification.

Figure 24. Illustration of matched filter rejection.

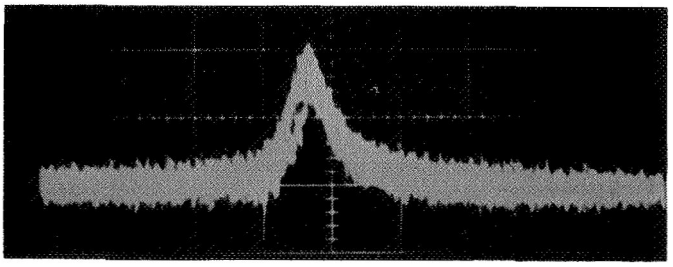

Vertical - 3.15 volts/div.

(a) Rectangular aperture autocorrelation (a' = 4mm)

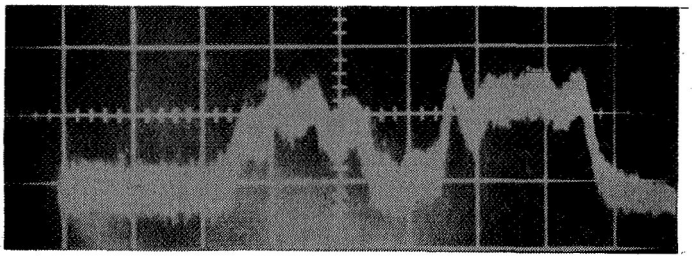

Vertical - 0.315 volts/div.

(b) Crosscorrelation between rectangular and circular aperture (2mm diameter).

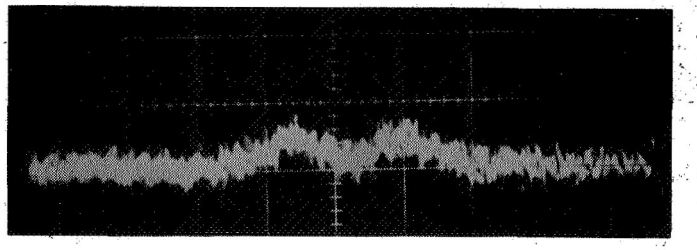

Vertical - 0.1 volts/div.

(c) Crosscorrelation between rectangular and circular aperture (0.5mm diameter).

Figure 25. Traces of correlation intensities from a filter matched to a 1 x 4mm rectangular aperture.

detection by means of matched filtering techniques. Further investigation in this area should include similar experimentation with the actual data transparencies.

# CHAPTER V

## AN OPTICAL DATA PROCESSOR FOR DETECTION AND STUDY OF METEOR TRAILS

The matched filter has been studied in considerable detail, including various aspects of selectivity or rejection characteristics, techniques for achieving relatively good filter diffraction efficiencies and requirements for input signal contrast. The results of these efforts will appear in this chapter in the form of specifications and design of an optical data processing system for detection and study of meteor trails. It is assumed that meteor trail information can be made available to the data processor by means of photographic film positive transparencies.

### Optical Configuration

A spherical wave matched filter optical correlator configuration is shown in Figure 26 and an analysis of this system is presented in Appendix B. Such a system is a practically useful one in that it provides a transform plane scaling capability, given by Equation B-2 as $1/\lambda d$. Hence, signal dimensions can be scaled (practically, scaling is accomplished by the parameter d) such that they match the filter even though the filter might have been made for a larger or smaller signal originally. This means that a

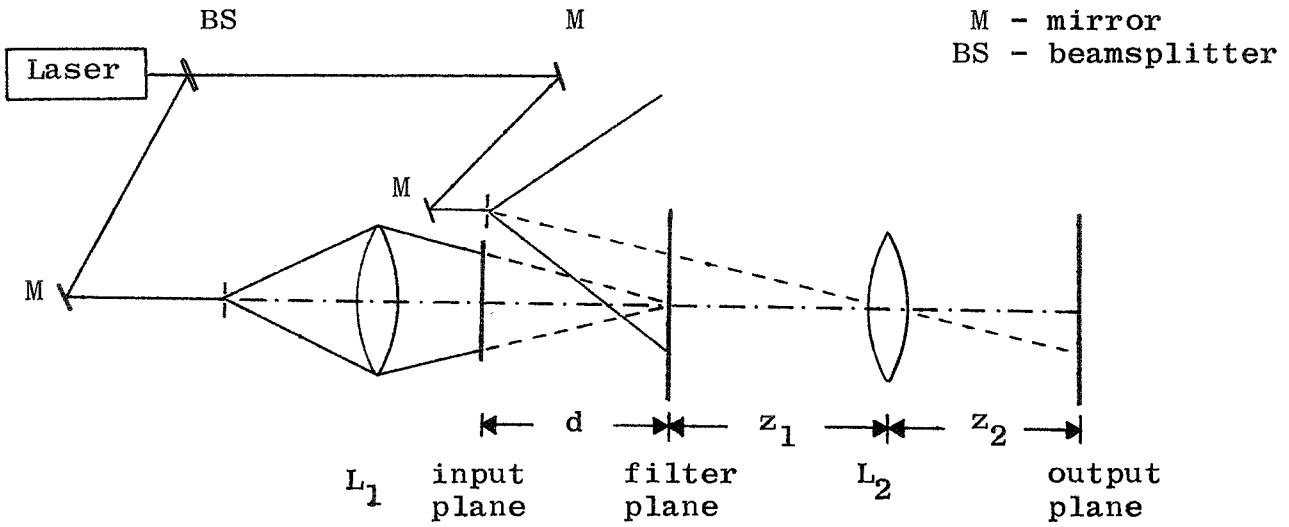


Figure 26. Spherical wave matched filter correlator configuration.

single filter can be employed to detect meteor trails which vary in size by changing the position of the lens $L_1$ relative to the filter plane.

Additional practical advantages are also offered by the spherical wave correlator. Lenses are a major source of noise in an optical system. A lens will amplitude and phase modulate an otherwise uniform light beam by means of pits, scratches, non-uniform coatings and etc. which are properties of most lenses. The spherical wave correlator design of Figure 26 utilizes only two lenses; thus, effects of lens noise are reduced, in addition to a reduction in costs of high quality lenses. With reference to the first transform operation (that due to $L_1$), effects of lens aberrations are reduced because this configuration allows lens operation to be restricted near the optical axis (compare this to the configuration of Figure A-1).

Besides the transform plane scale factor, an output plane scaling factor exists, as given by Equation B-9. This factor gives the relation between the output light distribution and the true distribution in cases where measurement of output distributions are required.

A limitation of the spherical wave configuration lies in the fact that the limiting aperture in the input plane varies with the distance d. A related factor is that the input plane illuminating intensity also varies with d. It

is thus necessary to design the system such that the beam diameter, input signal format and desired scaling range are compatible. It should also be noted that the output plane position is related to the transform plane scale factor by Equation B-11.

In addition to the basic components shown or implied by Figure 26, accessories such as translation stages, liquid gates and a bench mounted microscope are desirable. A microposition xy translation stage, on which the matched filter is mounted, and a bench mounted (with xyz positioning capability) microscope are useful in achieving the critical alignment of the filter. Liquid gates for the input and filter transparencies will produce a more intense, sharply focused light distribution in the output plane by making the filter operation less susceptible to phase shifts caused by variations in film emulsion thickness. The liquid gates are filled with a matching fluid which matches the index of refraction of the fluid to the emulsion, and should be employed in matched filter formation as well as the data processing step.

Data Input Considerations

It is assumed that meteor trail information would be introduced into the data processing system by way of photographic film positive transparencies. The transparencies could be in the form of a film roll which is fed through the

input plane (using a liquid gate preferably) frame by frame. As previously discussed, the matched filter is sensitive to rotational position; therefore, either the input plane or the filter plane must be rotated to accommodate trails with differing orientation. Recalling that the matched filter is shift-invariant, it would be practically easier to rotate the input plane. Rotation of the filter itself presents a mechanical design problem in that filter alignment is critical. Rotation would occur for each frame present in the input. Preferred meteor trail orientation or possible meteor trail symmetry would reduce the required amount of rotation to 180° or less. However, continuous rotation at a moderate rate is probably desirable from a design viewpoint.

Results of the contrast studies of Chapter IV show that input plane contrast has significant affect on detection in the output plane. The lower limit on contrast is dependent upon the methods employed in detection and readout. Experience with a TV type detector and video readout indicate that an input plane contrast value of approximately 2 is detectable. Additional work is required to determine characteristics of representative meteor trail data, including optimization of meteor trail recording processes.

The Matched Filter

Based upon results of the matched filter studies, two possible approaches can be taken to the meteor trail detection problem. First, the presence of a meteor trail in a particular frame can be detected with a relatively low S/R filter (S/R $\leq$ 2), assuming adequate input plane contrast. The low S/R filter is suggested here because of its relatively large output distribution (physical dimensions), the fact that such a filter exhibits modest selectivity characteristics for similar signals and its relatively good diffraction efficiency.

After a meteor trail has been determined to exist in a particular frame, that frame can be re-processed at a later time with a higher S/R filter (S/R $\simeq$ 30, or less) to determine more detailed properties of the meteor trail. Use of a higher S/R filter produces intense "spots" at each end of the correlation function and at the center (see Figure 8), which allows determination of the length of the trail relative to that for which the filter is matched. Also, in this step, the value of the output intensity can be measured and compared with that of meteor trails with known properties.

A second approach is to employ a relatively high ratio filter to detect and obtain detailed information concerning the properties of the detected meteor trail. In this case, it would probably be necessary to run the data several times

because the higher S/R filters are more selective and they will reject many meteor trails which are longer or shorter than that to which the filter is matched.

Output Detection and Readout

Detection of a correlation intensity distribution in the output plane which results from the presence of a meteor trail in the input requires that the appropriate portion of the output plane be searched (see Appendix A). Such a search can be carried out with a scanning photomultiplier tube or other such photosensitive device.

Another detection scheme utilizes a closed circuit television, providing a rapid electronic search of the output plane along with visual monitoring capability. A system similar to that described in Appendix C can be expanded to readout any desired data from the composite video, within the limits that the signal to noise ratio imposes. A limitation of the TV system lies in its limited dynamic range.

The output, however detected, can be related to a particular input frame, and even to the orientation producing the output. This would allow certain frames to be re-processed or otherwise examined; thus, discarding frames which do not contain meteor trails.

# CHAPTER VI

## CONCLUSIONS

The research efforts which have been reported upon here were directed towards development of coherent optical techniques applicable to detection and study of meteor trails. The coherent optical matched filter has been investigated both theoretically and experimentally for use in recognizing the presence of meteor trails, as recorded on photographic film positive transparencies, upon a background of star images.

Models of meteor trails employed in this work were long, narrow rectangular apertures. A matched filter model was used to determine filter selectivity and its output light distribution as a function of the bandpass characteristics of the filter. It was found that selectivity can be improved by blocking the transmission of light in the low frequency region of the filter. This high pass matched filter operation is useful when it is necessary to discriminate between similar signals; for example, such a technique would have important application in attempts to distinguish between meteor trails which only differ in length. Another effect of high pass matched filter operation upon meteor trails is to provide intense "spots" of light in the correlation light distribution which aids in the determination of meteor trail image dimen-

sions via correlation measurements.

Film processing for matched filter formation was studied. Determination of an optimum range of film density was made with regard to matched filter diffraction efficiency. In efforts to improve filter diffraction efficiencies, a bleaching step was added to the film processing procedure. It was found that the operation of bleached filters depends upon the signal to reference light component ratio during filter formation, as well as, the time of bleaching. These two factors determine the selectivity of bleached filters. In general, selectivity of a bleached filter is decreased as compared with that of the same unbleached filter, a result which is expected. Finally, an approximate relation was developed between the cut off frequency of a high pass matched filter and the signal to reference component ratio employed in filter formation.

Various other aspects of matched filter properties were considered relevant to operation of the filter in meteor trail detection. It was found that the meteor trail orientation requirements which allow recognition by a matched filter are a function of the signal to reference component ratio. That is, the higher values of signal to reference ratio produce a filter which is more sensitive to improper orientation of meteor trails in the input plane. It is necessary to provide an input plane rotational capability in order to accommodate trails with varying orientation.

One of the more important considerations with regard to application of the matched filter in meteor trail detection is that involving the contrast between the meteor trail and the input plane background. It was found that a portion of the light transmitted by the input plane background is diffracted into the output plane as a background for the correlation intensity. Results of experimentation relevant to this problem indicate that an input plane contrast of approximately 2 will yield a detectable output. However, this is obviously a function of the output detection scheme.

Matched filters can be made with sufficient selectivity to distinguish between similar signals. A filter which distinguishes between stars and meteor trails requires very modest selectivity characteristics. A spherical wave matched filter correlator configuration was presented and analyzed which offers a frequency plane scaling capability. This configuration is advantageous in meteor trail detection since a single matched filter can be employed to detect the presence of trails of differing sizes.

An output detection technique which was employed with considerable success in this reported work involved use of a closed circuit television system. This system provides a visual monitor, exhibiting a capability for rapid search of the output plane for revealing correlation intensity distributions. Electronic readout was effected by extracting desired

information from the composite video signal.

Actual meteor trail signal formats were not available for consideration during the period of time in which this research was conducted. All research efforts reported here were carried out using a rectangular aperture as a meteor trail model. The results of this work indicate that matched filter techniques developed here can be successfully employed for detection and study of meteor trails; however, further study is recommended, using actual meteor trail signal formats. Specifically, additional information concerning the characteristics of actual meteor trails is necessary. In this regard, refinement of the meteor trail model is desirable. In addition, determination of contrast requirements should be made for actual input signal formats.

# APPENDIX A

## DESCRIPTION AND ANALYSIS OF A MATCHED FILTER CORRELATOR

The system employed by Vander Lugt provides a means by which a complex filter can be made, recording both amplitude and phase information on a medium responsive to intensity (e.g., photographic film)(6). Formation of the matched filter can be described with the aid of Figure A-1. Collimated monochromatic light is made incident upon the input plane, which contains a signal to which the filter is to be matched. Let the input signal be represented in a two-dimensional coordinate system as $G(x_1,y_1)$, then the complex light amplitude distribution transmitted from the input plane is proportional to $G(x_1,y_1)$ and is collected by lens $L_1$. This lens provides a Fourier transformation of $G(x_1,y_1)$ in its back focal plane, $(x_2,y_2)$. The light amplitude distribution in plane $(x_2,y_2)$ is proportional to

$$\frac{1}{i\lambda f_1} \tilde{G}\left[\frac{x_2}{\lambda f_1}, \frac{y_2}{\lambda f_1}\right] \qquad \text{(A-1)}$$

where tilde denotes Fourier transformation. Here onward, $x_2/\lambda f_1 = u$ and $y_2/\lambda f_1 = v$ is defined.

In addition, as shown in Figure A-1, a second portion of the collimated light passes below the signal $G(x_1,y_1)$,

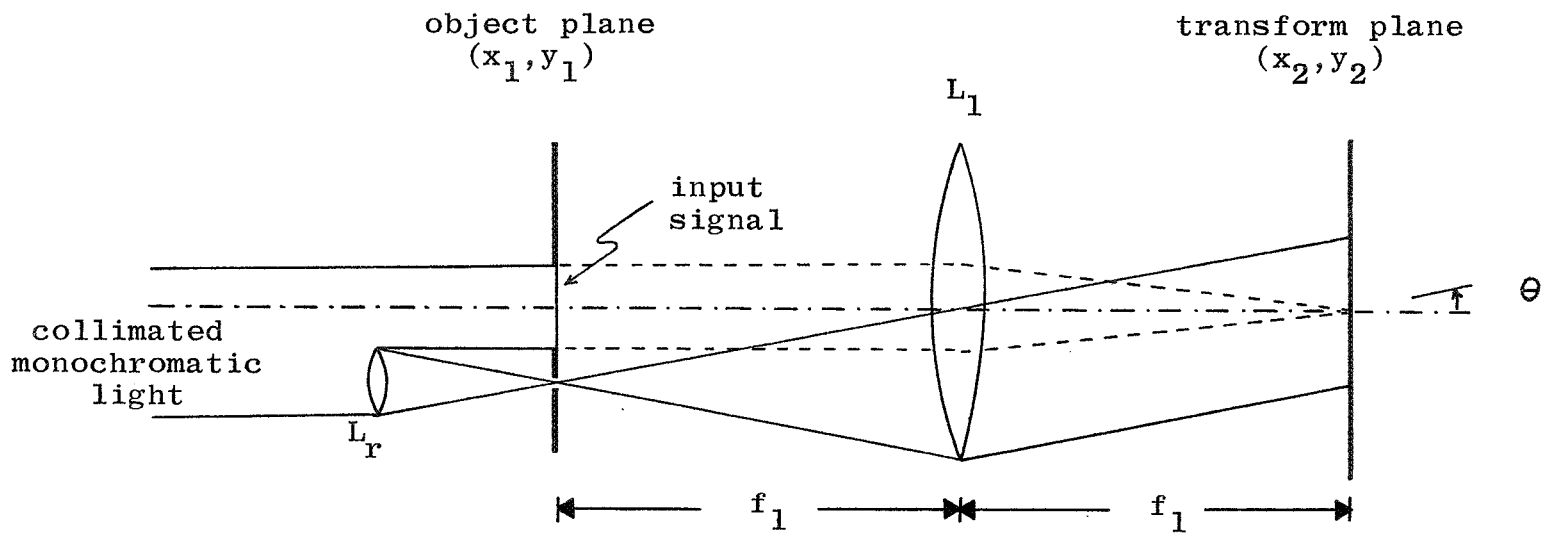


Figure A-1. Optical configuration for matched filter formation.

striking lens $L_r$ which focusses this light at the object plane and it is finally made incident on the back focal plane of lens $L_1$ with an inclination $\theta$ with respect to the optic axis. This beam is known as the reference beam. The tilted reference beam produces a light distribution in the transform plane which can be expressed as,

$$U_r(x_2,y_2) = A \exp(i2\pi\alpha y_2) \qquad \text{(A-2)}$$

where the spatial frequency $\alpha$ is given by

$$\alpha = \frac{\text{Sin } \theta}{\lambda}$$

and $\lambda$ is the wavelength of the laser light. Now, the total light amplitude distribution in plane $(x_2,y_2)$ can be written as

$$U(x_2,y_2) \propto [\tilde{G}(u,v) + A \exp(i2\pi\alpha y_2)] \qquad \text{(A-3)}$$

The total intensity incident upon the $(x_2,y_2)$ plane can be obtained from Equation A-3, and that is

$$I(x_2,y_2) = U(x_2,y_2)\ U^*(x_2,y_2) \qquad \text{(A-4)}$$

To make a matched filter, a photographic film is to

be exposed by placing it in the $(x_2,y_2)$ plane, taking note that the film responds to the optical intensity rather than the field amplitude. (Here, it is worth noting that the exposure time of the film should be selected properly according to the requirements as discussed in Chapter III.) The intensity to which the film is exposed can be written from Equation A-3 and A-4 as

$$I(x_2,y_2) \propto [\tilde{G}(u,v) + A \exp(i2\pi\alpha y_2)] \cdot [+ \tilde{G}^*(u,v) + A \exp(-i2\pi\alpha y_2)] \quad \text{(A-5)}$$

The transmittance of the film is proportional to $I^{-\gamma/2}$, and by making the slope of the Hurter-Driffield curve, $\gamma$, equal minus two (i.e., a photographic positive) the desired linear relation between signal amplitude during exposure and light amplitude transmittance of the film can be achieved. In practice, the reference light amplitude is made much greater than that of the signal throughout the band pass region of the filter (small signal conditions) to yield an amplitude transmittance

$$T(x_2,y_2) \propto A^2 - \frac{\gamma}{2}\left[\frac{1}{(\lambda f_1)^2}|\tilde{G}(u,v)|^2 + A\tilde{G}^*(u,v) \times \exp(i2\pi\alpha y_2) + A\tilde{G}(u,v)\exp(-i2\pi\alpha y_2)\right] \quad \text{(A-6)}$$

The binomial expansion is used to obtain Equation A-6 and terms of higher order than one are dropped. The resulting film (Fourier transform hologram) can be utilized as a matched filter.

Input Data Processing

With the above matched filter, the input data can be processed as shown in Figure A-2. In data processing, the reference beam is blocked, the filter is placed in the back focal plane of lens $L_1$ and an additional lens $L_2$ having a focal length $f_2$ is introduced to the system as shown in Figure A-1.

Consider that a signal format described by $S(x_1,y_1)$ is placed into the input plane. A field distribution proportional to $\tilde{S}(u,v)$ is incident upon the matched filter as lens $L_1$ provides the Fourier transform of the signal format in its back focal plane. The light amplitude transmitted by the filter can be described from Equations A-1 and A-5 as,

$$\begin{aligned} T(x_2,y_2) \propto\ & \tilde{S}(u,v)\ \tilde{G}(u,v)\ \tilde{G}^*(u,v) \\ & + A^2\ \tilde{S}(u,v) + A\ \tilde{S}(u,v)\ \tilde{G}(u,v) \\ & \times \exp(-i2\pi\alpha y_2) + A\ \tilde{S}(u,v)\ \tilde{G}^*(u,v) \\ & \times \exp(i2\pi\alpha y_2) \end{aligned} \qquad \text{(A-7)}$$

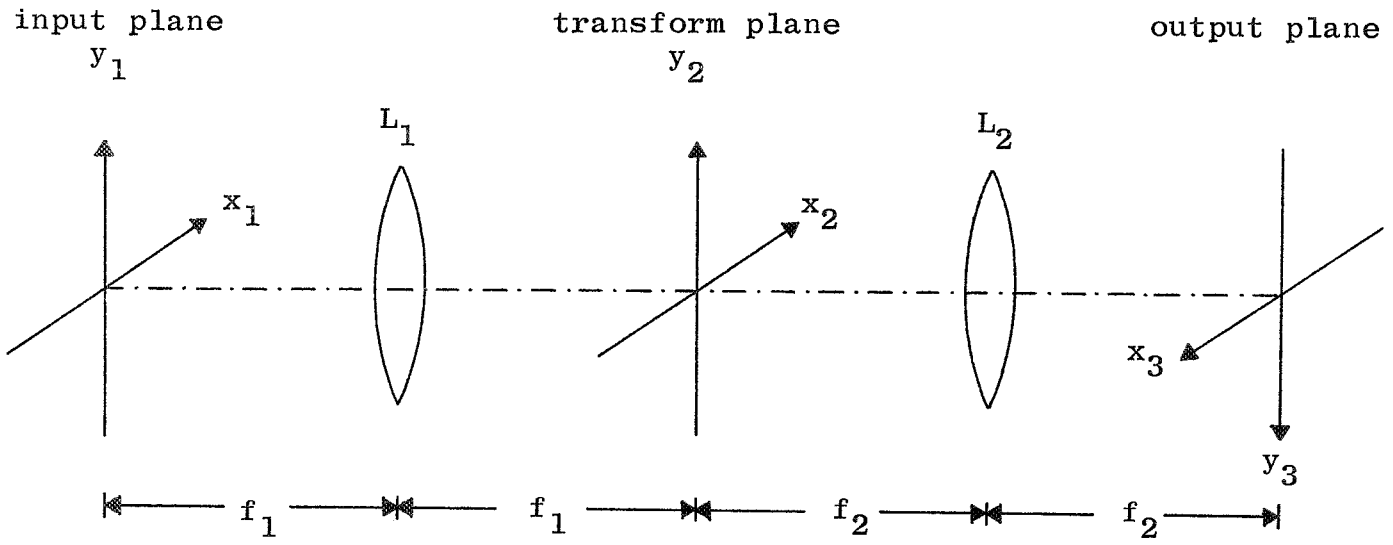


Figure A-2. Optical configuration for matched filter operation.

Considering the individual terms of Equation A-7, the first two terms correspond to light distributions centered on the optic axis in plane $(x_3,y_3)$. The last two terms correspond to light distributions located at positions on opposite sides of the optic axis, displaced according to $\pm\theta$. Of the latter terms, the third term represents a convolution operation, while the last term is the correlation operation as it represents the conjugate of $G(x_1,y_1)$. Here onward in the analysis, only the last term is considered.

Lens $L_2$ collects the filter transmitted light corresponding to the last term of Equation A-7, and performs a Fourier transform on this amplitude function. The transformation results in a complex light amplitude distribution in the back focal plane of lens $L_2$, which can be expressed by convolution notation (taking note of the reflected coordinates $(x_3,y_3)$ as shown in Figure A-2) and letting $f_1 = f_2 = f$.

$$\Phi(x_3,y_3) \propto \int_{-\infty}^{\infty}\int_{-\infty}^{\infty} \tilde{S}(u,v)\,\tilde{G}^*(u,v)\,\exp\{-2\pi i[x_3u + (y_3-\alpha\lambda f)v]\}\,dudv \tag{A-8}$$

$$\Phi(x_3,y_3) \propto S(x_3,y_3) \circledast G^*(-x_3,-y_3) \circledast \delta(x_3,y_3 + \alpha\lambda f),$$

and also

$$\Phi(x_3,y_3) \propto \int_{-\infty}^{\infty}\int_{-\infty}^{\infty} S(\xi,\eta)\; G^*(\xi - x_3, \eta - y_3 - \alpha\lambda f)\,d\xi d\eta, \tag{A-9}$$

which is the crosscorrelation of G and S centered at coordinates $(0, -\alpha\lambda f)$ in $(x_3, y_3)$ plane.

The term $-\alpha\lambda f$, in the argument of the complex exponential of Equation A-8, and in the argument of G* of Equation A-9, serves to translate the output correlation component light distribution off-axis. Since this term does not affect the light distribution, it is not included in the expressions in the text, nor in figures and diagrams, for reasons of brevity. In practice, the value of $\alpha$ must be selected such that the correlation light distribution does not overlap or interfere with the light distribution existing on-axis in the output plane (2).

# APPENDIX B

## ANALYSIS OF THE SPHERICAL WAVE MATCHED FILTER CORRELATOR

The spherical wave coherent optical Fourier transform configuration is a practically useful one in that it provides a transform plane scaling capability. Incorporating this scheme in a matched filter correlator as proposed by Vander Lugt (11) offers additional advantages. The configuration as depicted by Figure 26 does not require a collimating lens; thus, the cost is reduced and a major source of system noise is removed. In addition, lens operation can be restricted near the optic axis where aberrations are minimized.

In the analysis to follow, the system limiting apertures are assumed to be sufficiently large to accommodate all input signal formats of interest. Thus, with reference to Figure 26, it can be shown that the light amplitude distribution incident upon the input plane $(x_1,y_1)$ may be expressed by (2)

$$U(x_1,y_1) = K \exp[- i \frac{k}{2d} (x_1^2 + y_1^2)] \qquad \text{(B-1)}$$

Here, it is assumed that a monochromatic source of light with wavelength $\lambda$ is collected by lens $L_1$ which has a focal length $f_1$, and $k = 2\pi/\lambda$. An input signal format whose amplitude

transmittance is $S(x_1,y_1)$ is Fourier transformed and mixed with a reference light amplitude $(A/j\lambda d)\exp(-j2\pi\alpha y_2)$ to yield an amplitude distribution in the $(x_2,y_2)$ plane given by

$$U^{-}(x_2,y_2) = \frac{1}{i\lambda d}\exp\left[i\ \frac{k}{2d}\ (x_2^{\,2} + y_2^{\,2})\right]$$
$$\cdot\ \{A\ \exp(-\ i2\pi\alpha y_2) + K\tilde{S}(\frac{x_2}{\lambda d},\ \frac{y_2}{\lambda d})\} \qquad \text{(B-2)}$$

where $\alpha = \sin\theta/\lambda$ and tilde denotes Fourier transformation. The transform plane scaling factor, $1/\lambda d$, is noted in the above expression. A photographic film exposed to the intensity corresponding to this amplitude distribution is processed and returned to the $(x_2,y_2)$ plane to function as a matched filter. The quadratic phase factor is seen to cancel here when intensity is considered, due to the location of the reference point source in the input plane.

Blocking the reference light, a new input signal format described by $G(x_1,y_1)$ is placed in the input plane. The light amplitude distribution incident upon the filter becomes

$$\frac{K}{i\lambda d}\exp\left[i\ \frac{k}{2d}\ (x_2^{\,2} + y_2^{\,2})\right]\tilde{G}(\frac{x_2}{\lambda d},\ \frac{y_2}{\lambda d}) \qquad \text{(B-3)}$$

The amplitude component transmitted by the filter which is of primary interest in matched filter correlation is

$$U^{+}(x_2,y_2) = \frac{1}{i\lambda d} KA^2 \exp[i \frac{k}{2d}(x_2^2 + y_2^2)]$$

$$\cdot \tilde{G}(\frac{x_2}{\lambda d}, \frac{y_2}{\lambda d}) \tilde{S}^{*} (\frac{x_2}{\lambda d}, \frac{y_2}{\lambda d}) \exp(- i2\pi\alpha y_2) \qquad \text{(B-4)}$$

and the proportionality constant associated with the film is set to unity for convenience.

The lens $L_2$ performs a Fourier transformation upon the amplitude distribution transmitted by the filter. The desired results could be written immediately except for the presence of the multiplicative quadratic phase factor. Because of this factor, it is necessary to determine its affect upon the transform operation. That is, determination of the plane in which the transform exists must be made. Use of the Fresnel diffraction formula shows the output amplitude distribution to be

$$U(x_3,y_3) = \frac{KA^2}{(\lambda d)^2} \exp\{i \frac{k}{2z_2}[1 - \frac{z_1 f_2}{\sigma}](x_3^2 + y_3^2)\}$$

$$\cdot \int_{-\infty}^{\infty} \int_{-\infty}^{\infty} \tilde{G}(\frac{x_2}{\lambda d}, \frac{y_2}{\lambda d}) \tilde{S}^{*} (\frac{x_2}{\lambda d}, \frac{y_2}{\lambda d}) \exp\{i \frac{k}{2}[\frac{-f_2 z_2}{\sigma} + \frac{1}{d} + \frac{1}{z_1}]$$

$$\cdot (x_2^2 + y_2^2)\} \exp(- i2\pi\alpha y_2)$$

$$\cdot \exp\{- i \frac{kf_2}{\sigma} (x_2 x_3 + y_2 y_3)\} dx_2 dy_2 \qquad \text{(B-5)}$$

where $\sigma = f_2(z_1 + z_2) - z_1 z_2$.

In order for the output light distribution to focus in a plane and provide the desired Fourier transformation, the quadratic phase factor within the integrand must be made equal to unity. This is accomplished when

$$z_2 = \frac{f_2(z_1 + d)}{(z_1 + d) - f_2} \tag{B-6}$$

Normally, the output intensity is required (i.e., the correlation intensity), and the quadratic phase factor outside the integral in Equation B-5 is unimportant. However, it too can be made equal to unity by letting

$$z_1 = f_2 \tag{B-7}$$

In this case, the light amplitude distribution in the output plane is proportional to the Fourier transform of $\tilde{\tilde{G}}S^*$ centered off-axis. In either case, the output correlation intensity is given by

$$|U(x_3, y_3)|^2$$

$$= \left| KA^2 \int_{-\infty}^{\infty} \int_{-\infty}^{\infty} G[\epsilon\xi, \epsilon\eta] S^*[\epsilon(\xi - x_3), \epsilon(\eta - y_3) + \alpha\lambda d] d\xi d\eta \right|^2 \tag{B-8}$$

where

$$\epsilon = \frac{f_2 d}{\sigma} \tag{B-9}$$

is the output plane scaling factor. Under the conditions of Equation B-6, this scaling factor becomes

$$\epsilon = \frac{z_1 + d - f_2}{f_2} \tag{B-10}$$

If the conditions of Equation B-7 are adopted, the location of the output plane relative to lens $L_2$ is given by

$$z_2 = \frac{f_2(f_2 + d)}{d} \tag{B-11}$$

and the output plane scaling factor becomes

$$\epsilon = \frac{d}{f_2} \tag{B-12}$$

Of practical importance is the fact that the proper location of the output plane is that position where the reference point source image appears, in the absence of any obstruction in the filter plane. This can be seen by considering the lens equation for $L_2$;

$$\frac{1}{f_2} = \frac{1}{d + z_1} + \frac{1}{z_2} \qquad \text{(B-13)}$$

thus gives a reference point source image distance $z_2$ identical to Equation B-6. The relations of Equations B-6 and B-10 are depicted by Figure B-1.

It has been shown that the location of the output plane is dependent upon the position of the input plane and second transform lens relative to the filter plane. Also, in addition to the filter plane scale factor, an output plane scaling factor has been determined.

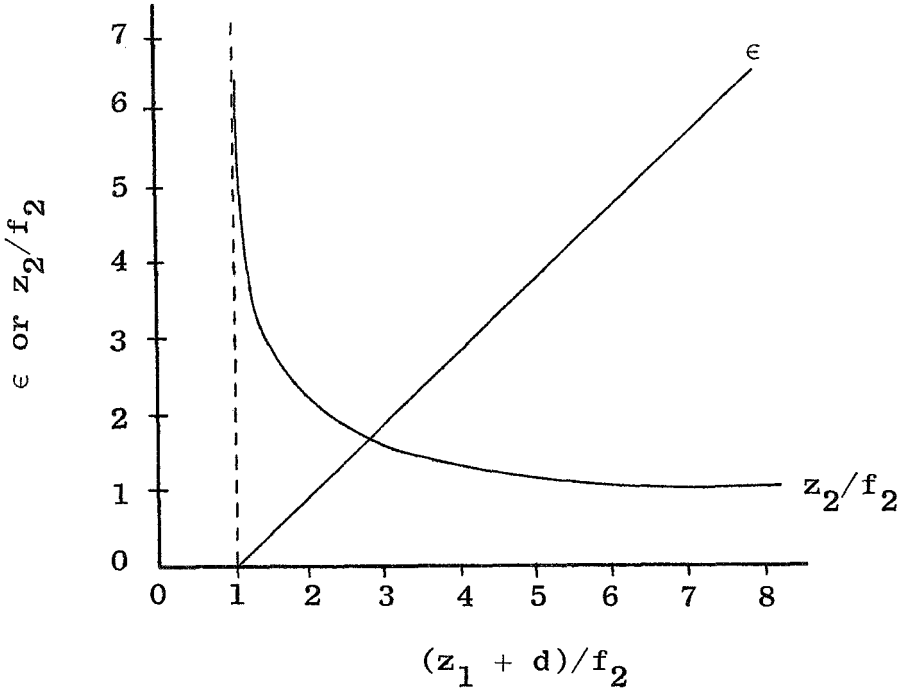


Figure B-1. Relationships between system parameters and output plane position and scale factor.

# APPENDIX C

## CLOSED CIRCUIT TELEVISION LINE SCANNER

A closed circuit television system can be adapted to provide an analog voltage readout while maintaining visual monitoring capability. The analog voltage may be presented on an oscilloscope CRT (or otherwise processed), the voltage being proportional to the intensity incident upon the Vidicon. A system is described here which allows isolation of one horizontal scan line, or a portion of one scan line, from which the video signal may be extracted. Such a system is most easily realized through the use of an oscilloscope with a delayed sweep function. However, it is necessary to obtain syncronization pulses from the camera in order to syncronize the oscilloscope. If a sync pulse output is not available from the camera, it can be extracted from the composite video output of the camera. A circuit which can be used for such is shown in Figure C-1. Use of this circuit makes it unnecessary to make connections internal to the camera and permits use of the line scanner technique with different cameras.

### Sync Recovery Circuit

With reference to Figure C-1, composite video signals enter transistor $Q_1$ and are amplified; the signal is then DC restored at its output. Transistor $Q_2$ removes the picture

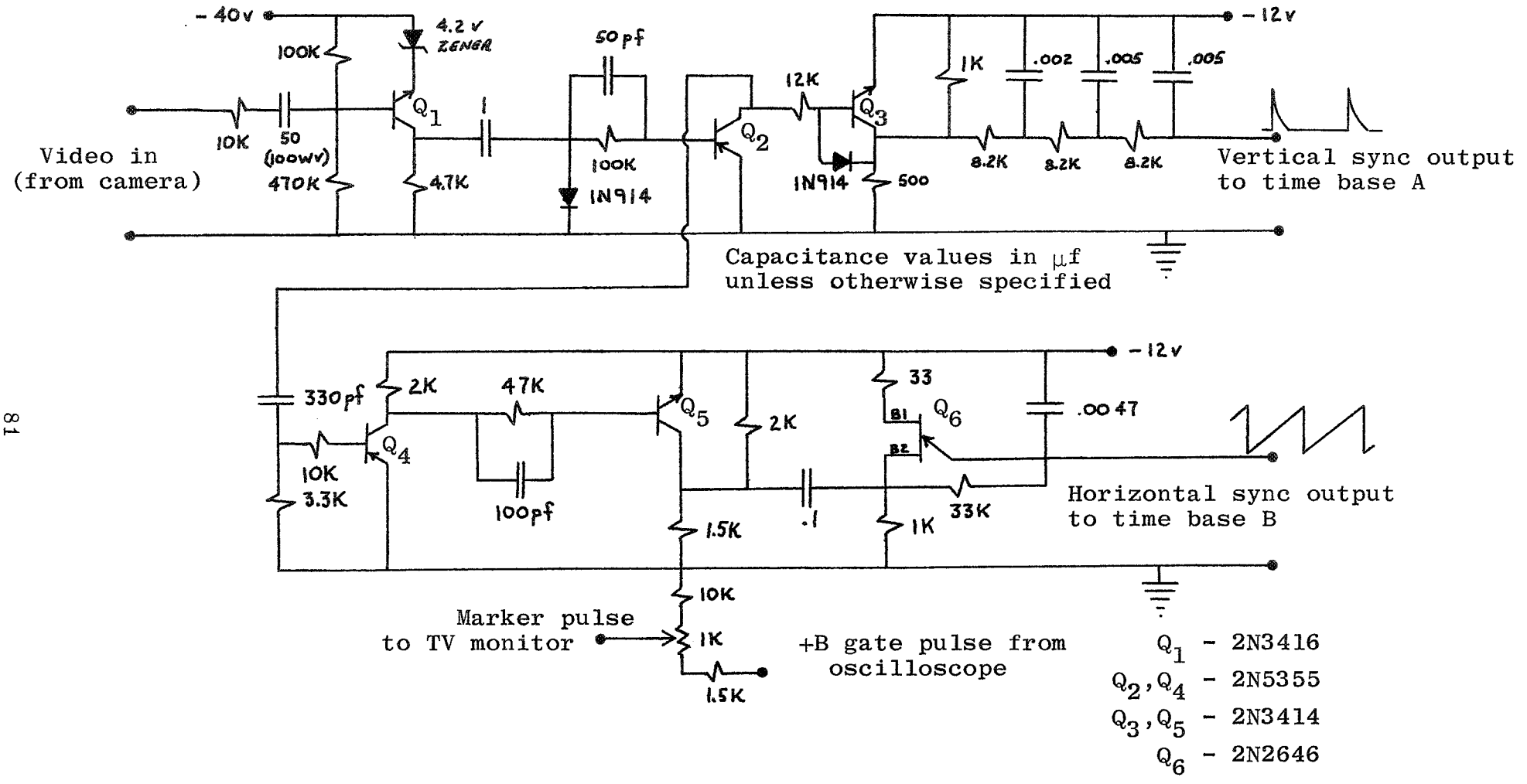


Figure C-1. Sync Recovery Circuit.

information, and, due to the low pass characteristics of $Q_3$ and its circuitry, only the vertical sync pulses reach the vertical sync signal output. From $Q_2$ the horizontal sync pulses are separated by a differentiator circuit which includes transistor $Q_4$. Transistor $Q_5$ inverts the signal which is then used to synchronize a unijunction ($Q_6$) sawtooth wave generator with the horizontal sync pulses from the camera. The sawtooth signal constitutes one trigger source to be used by the oscilloscope, the vertical sync pulse from $Q_3$ the other.

In addition to the recovery of the sync signals there is a divider network that allows the use of a gate pulse from the oscilloscope to produce a white line marker for the television monitor, thus facilitating data location. This marker is used to locate the position of the scan line from which data is read out via the oscilloscope.

Set-up and Test Procedure

The following is a setup and operation procedure for the line scanner system. Although the procedure is for the sync pulse recovery circuit used with the type 555 Tektronix dual beam oscilloscope equipped with a 21-A (time base A) and a 22-A (time base B) plug in unit, the test set-up should be applicable to most oscilloscopes with delayed sweep capabilities. This delayed sweep function is used to isolate and expand the desired portion of the video signal to be studied.

1. The composite video signal from the camera is applied to the input of the sync pulse recovery circuit and to channel one of the oscilloscope.
2. The "A" time base is set to trigger on either positive or negative going slope and uses the vertical sync pulse output from the sync pulse recovery circuit as an external trigger source. The useful ranges of "A" sweep times were 5, 2, and 1 milli sec./cm. The trigger vernier is set to provide a stable trace of the composite video.
3. The "B" time base is set to trigger on the positive slope of the sawtooth output of the recovery circuit. The sawtooth wave rises from its valley to its peak during one horizontal scan by the television so that by oscilloscope "B" trigger vernier adjustment any convenient trigger point along a horizontal scan line can be obtained. The positive "B" time base gate pulse output from the oscilloscope is fed to the divider network to provide a marker for the television monitor. The "B" time base is useful in the .5 to .1 $\mu$ sec/cm sweep ranges.
4. The "B" trigger vernier provides the means by which location of any portion of a horizontal scan line to be expanded and observed is obtained. In practice

the marker line seen on the television monitor is the portion being read by the oscilloscope. The marker line position can be adjusted to the left of the screen by the "B" time base course trigger vernier and is shifted to the right along the horizontal scan line by the fine trigger vernier adjustment. The delay vernier control on the oscilloscope is used for the choice of the particular horizontal line to be observed.

Prior to the use of the line scanner system described above, the dynamic characteristics of the TV camera employed should be determined. This information provides a knowledge of the linear range of operation for such a system.

# APPENDIX D

## DEVELOPMENT OF BANDLIMITED RECTANGULAR APERTURE CORRELATION FUNCTION

The output correlation light amplitude distribution can be found by substitution of Equations 6 and 8 into Equation 4 of Chapter II. In order to simplify the mathematical manipulations involved, use is made of the fact that the substitution results in a separable function. Thus, the two-dimensional problem can be handled as two one-dimensional problems, the two dimensional result being the product of the two one-dimensional results.

In one-dimension, Equation 4 becomes

$$\Phi(x_3) \propto 2\, aa' \int_{m'}^{m} \operatorname{sinc}(\pi a u)\, \operatorname{sinc}(\pi a' u) \cos(2\pi u x_3)\, du. \quad \text{(D-1)}$$

Using trigonometric identities, the above expression can be integrated to give

$$\Phi(x_3/a') \propto \frac{a'}{2\pi} \frac{1}{\pi a' m} \left[ -\cos(p_1 \pi a' m) - \cos(p_2 \pi a' m) \right.$$

$$\left. + \cos(p_3 \pi a' m) + \cos(p_4 \pi a' m) \right] + \frac{1}{\pi a' m'} \left[ \cos(p_1 \pi a' m') \right.$$

$$\left. + \cos(p_2 \pi a' m') - \cos(p_3 \pi a' m') - \cos(p_4 \pi a' m') \right]$$

$$-p_1 \left[ \mathrm{Si}(p_1 \pi a' m) - \mathrm{Si}(p_1 \pi a' m') \right] - p_2 \left[ \mathrm{Si}(p_2 \pi a' m) - \mathrm{Si}(p_2 \pi a' m') \right]$$

$$+p_3 \left[ \mathrm{Si}(p_3 \pi a' m) - \mathrm{Si}(p_3 \pi a' m') \right] + p_4 \left[ \mathrm{Si}(p_4 \pi a' m) - \mathrm{Si}(p_4 \pi a' m') \right] , \quad \text{(D-2)}$$

where

$$p_1 = 1 - a/a' - 2x_3/a'$$
$$p_2 = 1 - a/a' + 2x_3/a'$$
$$p_3 = 1 + a/a' - 2x_3/a'$$
$$p_4 = 1 + a/a' + 2x_3/a'$$

The sine integral appearing above is a tabulated function defined as

$$\mathrm{Si}(x) = \int_0^x \frac{\sin(z)}{z} \, dz$$

The expression for the one-dimensional correlation light amplitude distribution given by Equation D-2 is quite general. It may be employed to calculate both autocorrelation and crosscorrelation distributions for wideband and various band-

limited matched filters. It should be noted that $a/a' = 1$ gives autocorrelation and $a \neq a'$ crosscorrelation (see Figure 3). The cut off frequencies $m'$ and $m$ (see Figure 2) for these filters are as follows:

Wideband filter: $m' = o$

$m = \infty$

Low pass filter: $m' = o$

$m$ = prescribed upper cut off frequency

High pass filter: $m'$ = prescribed lower cut off frequency

$m = \infty$

Band pass filter: $m'$ = prescribed lower cut off frequency

$m$ = prescribed upper cut off frequency

Further examination of Equation D-2 reveals that normalized correlation distributions can be depicted in terms of $\Phi(x_3/a')/a'$, as a function of $x_3/a'$. The normalized cut off frequencies are then $a'm'$ and $a'm$.

A one-dimensional problem has been solved above. The expression for the second one-dimensional correlation amplitude distribution is similar to Equation D-2. The distribution $\Phi(y_3/b')$ is obtained by changing $x_3, a', a, m'$ and $m$ to

$y_3$,b′,b,n′ and n, respectively, in Equation D-2. Thus, for the rectangular aperture signal format, the two one-dimensional distributions differ by only a scale factor. Finally, the two dimensional correlation amplitude distribution is given by

$$\Phi\left[\frac{x_3}{a'}, \frac{y_3}{b'}\right] = \Phi\left[\frac{x_3}{a'}\right] \Phi\left[\frac{y_3}{b'}\right] . \qquad \text{(D-3)}$$

Data are presented in the text corresponding to one-dimensional curves (e.g., $y_3/b' = 0$) of correlation intensity, which is the detectable output quantity. These data represent

$$\left| \Phi(x_3/a')/a' \right|^2$$

# APPENDIX E

## IMPROVED DIFFRACTION EFFICIENCY OF MATCHED FILTERS BY CHEMICAL BLEACHING

The coherent optical matched filter is a Fourier transform type hologram of the signal to which the filter is matched. Several authors have theoretically predicted that the diffraction efficiency of simple plane wave holograms may be increased by chemically bleaching the hologram ( 12, 13, 14, 15, 16 ). The chemical bleaching of amplitude holograms produces phase holograms, the difference between the two types of holograms being that an amplitude hologram is recorded on photographic film as an absorption grating, whereas the phase hologram is recorded as an index of refraction grating. Theory predicts that the maximum diffraction efficiency of an absorption type hologram is 6.25% (2); in practice, the efficiency values achieved are generally lower than this value. In contrast to these relatively low efficiency values of absorption holograms, one author has shown theoretically that the diffraction efficiency of phase holograms should approach 100% (12). Here again, this theoretical value probably cannot be obtained in practice. However, the two theoretical values do indicate the large potential increase in diffraction efficiency for phase holograms. Since the coherent optical matched

filter is in reality a Fourier transform hologram, it would seem that the bleaching process might be applicable to the matched filter.

In this study, matched filters are made for the rectangular aperture meteor trail model on Kodak 649F spectroscopic plates and bleached in a potassium ferricyanide solution. The purpose of this work is to demonstrate the feasibility of bleaching matched filters, and to determine the effects of bleaching upon matched filter operation.

## Theory of Bleaching

As stated previously, phase holograms have the potential for achieving much greater diffraction efficiencies than amplitude holograms. One convenient method of producing a phase hologram is by first making an amplitude hologram and then bleaching it with an appropriate chemical solution. Because such holograms operate on the phase rather than the amplitude of the incident light wave, it is necessary to find a bleaching material which will leave the hologram completely transparent (14). Phase modifications to the incident beam will then be caused by an index of refraction variation in the emulsion.

During the exposure and development of an amplitude hologram, the silver halide particles of the film emulsion

are converted to silver; a fixing step follows, during which the unexposed silver halide particles are removed from the emulsion, leaving the silver image. To change the amplitude hologram to a phase hologram, the silver sites are converted to a transparent compound which has an index of refraction different from that of the emulsion.

The mathematical development of the absorption type matched filter is given in Appendix A, where an expression for the transmittance of the amplitude filter is given by Equation A-6. In general, the transmittance of a hologram may be expressed as an amplitude and a phase; thus,

$$T(x_2,y_2) \propto t_o \exp[i\phi(x_2,y_2)].$$

When dealing with an amplitude hologram, the transmittance function is ideally a real function, and the phase is equal to zero; this ideal case was assumed in the development of Equation A-6. When the amplitude hologram is bleached, the amplitude variations are removed and $t_o$ approaches unity (i.e., the hologram is transparent). Thus, the transmittance of the bleached hologram (or matched filter) can now be expressed as

$$T(x_2,y_2) \propto \exp[i\phi(x_2,y_2)],$$

where the phase variation $\phi\ (x_2,\ y_2)$ has been introduced as

a result of the index of refraction grating $n(x_2, y_2)$ created by the bleaching process (17). The variation in $n(x_2, y_2)$ for the bleached hologram is approximately proportional to the mass of silver which was originally exposed in making the amplitude hologram; in other words, the more silver sites which were originally exposed, and were then converted to a transparent material, the greater the change in index of refraction (14). Thus, absorption holograms which have high original densities give the greatest index of refraction variation after bleaching. Now, the density of the absorption hologram is proportional to the intensity during exposure; thus, since $\phi(x_2, y_2)$ is proportional to $I(x_2, y_2)$, we may express the transmittance of the bleached hologram as

$$T(x_2,y_2) \propto \exp[iI(x_2,y_2)].$$

The intensity incident upon the film during matched filter formation may be written as

$$I(x_2,y_2) \propto A^2 + |\tilde{G}(u,v)|^2 + 2A|\tilde{G}(u,v)| \cos[2\pi\alpha y_2 - \Psi],$$

where

$$\tilde{G}(u,v) = |\tilde{G}(u,v)| \exp[i\Psi(u,v)].$$

Finally, the transmittance becomes

$$T(x_2,y_2) \propto \exp\{i[A^2 + |\tilde{G}(u,v)|^2]\}\exp\{i[2A|\tilde{G}(u,v)| \cos(2\pi\alpha y_2 - \Psi)]\}.$$

Thus, we see that the transmittance of a bleached hologram is ideally a pure phase quantity.

To emphasize the concept of the refractive index grating caused by bleaching the amplitude hologram, we may express $\phi(x_2, y_2)$ as

$$\phi(x_2,y_2) \propto n_o + n_1 \cos(2\pi\alpha y_2 - \Psi),$$

where $n_o$ is the average index of refraction across the emulsion and $n_1$ is one-half the maximum change in the refractive index. To minimize distortion in the optical output of the bleached matched filter, the phase modulation should be kept small.

Bleaching Chemicals

A wide variety of materials have been investigated as possible bleaching agents for the production of phase holograms. Among the bleaches most often used are mercuric chloride ($HgCl_2$), Kodak Chromium Intensifier Bleach, potassium ferricyanide ($3K_3Fe(CN)_6$), cupric bromide ($CuBr_2$), and the so-called R-10 bleaches. It is generally agreed that the chemical reactions that occur with the silver particles during bleaching are the following (12,13,14,15,16):

1. Mercuric Chloride

$$Ag + HgCl_2 \rightarrow AgCl\ HgCl$$

2. Potassium Ferricyanide

$$Ag + K_3Fe(CN)_6 + KBr \rightarrow AgBr + K_4Fe(CN)_6$$

3. Copper Bromide

$$2Ag + CuBr_2 + H_2O_2 \rightarrow 2AgBr + H_2O_1 + CuO$$

4. R-10 Bleach

$$9Ag + 12NaCl + 7H_2SO_4 + (NH_4)_2Cr_2O_7 \rightarrow$$
$$9AgCl + Cr_2Cl_3 + 7H_2O + 6Na_2SO_4 + (NH_4)_2SO_4.$$

The Kodak Chromium Intensifier Bleach probably has a reaction equation similar to that of the R-10 bleach, since they both contain $Cr_2O_7$ with either ammonium $(NH_4)_2$ or some other compound.

As can be seen from each of the above reaction equations, each bleach reacts with the silver of the amplitude hologram to produce an insoluble transparent compound; thus, the resultant hologram is left transparent. In bleaching the amplitude hologram, it is necessary to make the hologram as transparent as possible so as to convert the hologram to a pure phase hologram.

Each of the bleaches mentioned above has certain desirable properties. For example, the mercuric chloride bleach often produces phase holograms which have greater diffraction efficiencies than those of the other bleaches. However, mercuric chloride bleach forms compounds that are unstable and which have a tendency to become more opaque with exposure to light (16). Thus, an additional processing step

is necessary after bleaching to make the emulsion stable; it has been found that by soaking the bleached plates in a solution of a mercuric halogen they become more stable. Another factor to be considered concerning mercuric chloride bleach is the fact that mercuric compounds present a certain safety hazard, as they may be absorbed through the skin.

The copper bromide bleaches also give good diffraction efficiencies; however, like mercuric chloride phase holograms, holograms produced by copper bromide are unstable without further processing after the bleaching step.

The potassium ferricyanide solutions are very appealing as potential bleaching agents. Unlike mercuric chloride, potassium ferricyanide presents no safety hazards. A second advantage of potassium ferricyanide is that it produces phase holograms which are stable without further processing. It is true that potassium ferricyanide produces diffraction efficiencies that are somewhat lower than those produced by mercuric chloride; however, if one is willing to accept the small decrease in diffraction efficiency associated with potassium ferricyanide, he gains the increased ease of handling and stability of the bleached plates.

BIBLIOGRAPHY


1. Andrews, H. C., Computer Techniques in Image Processing, Academic Press, New York, 1970.

2. Goodman, J. W., Introduction to Fourier Optics, McGraw-Hill Book Co., New York, 1968.

3. Vander Lugt, et. al., "Character Reading by Optical Spatial Filtering," Optical and Electro-Optical Information, J. Tippett, et al., editors, Cambridge, Massachusetts Institute of Technology Press, 1966.

4. Khol, R. "Optical Computers," Machine Design, 41:117, Aug. 21, 1969.

5. Marom, E. "Early Warning of Material Fatigue," Laser Focus, 5:43, Oct., 1969.

6. Vander Lugt, A. B. "Signal Detection by Complex Spatial Filtering," IEEE Transactions on Information Theory, IT-10:139-145, April, 1964.

7. Gee, T. H., and W. Linton, Jr. "Some Aspects of Band Limiting in Coherent Optical Matched Filtering," Instrumentation in the Aerospace Industry, 16:126-130, 1970.

8. Frecska, S. A., "Characteristics of Agfa-Gevaert Type 10E70 Holographic Film," Applied Optics, 7:2312-2314, Nov. 1968.

9. Pernick, B. J., et. al., "Film Transmittance-Exposure Characteristics for 649F at 6328 Å," Applied Optics, 7:714-715, April 1968.

10. Cody, R. L., "Various Coherent Optical Filtering Operations," M.S. Thesis, Univ. of Tennessee, Mar. 1971.

11. Vander Lugt, A., "Practical Considerations for the Use of Spatial Carrier-Frequency Filters," Applied Optics, 5:1760-1765, Nov. 1966.

12. Burckhardt, C. B., and E. T. Doherty. "A Bleach Process for High-Efficiency Low-Noise Holograms," Applied Optics, 8:2479-2482, Dec., 1969.

13. Upatnieks, J., and C. Leonard. "Efficiency and Image Contrast of Dielectric Holograms," Journal of the Optical Society of America, 60:297-302, Mar. 1970.

14. Latta, J. N. "The Bleaching of Holographic Diffraction Gratings for Maximum Efficiency," Applied Optics, 7:2409-2416, Dec., 1968.

15. Burckhardt, C. B. "Efficiency of a Dielectric Grating," Journal of the Optical Society of America, 57:601-603, May, 1967.

16. Upatnieks, J., and C. Leonard. "Diffraction Efficiency of Bleached, Photographically Recorded Interference Patterns," Applied Optics, 8:85-89, Jan., 1969.

17. Smith, H. M., Principles of Holography, John Wiley and Sons, Inc., New York, 1969.



MSFC—RSA, Ala